Materials Horizons

ROYAL SOCIETY OF CHEMISTRY

REVIEW

View Article Online
View Journal | View Issue

Cite this: *Mater. Horiz.*, 2022, **9**, 121

Design strategies for improving the crystallinity of covalent organic frameworks and conjugated polymers: a review

Jie Yang,†[a] Fangyuan Kang,†[a] Xiang Wang[a] and Qichun Zhang *[ab]

Received 20th May 2021,
Accepted 19th July 2021

DOI: 10.1039/d1mh00809a

rsc.li/materials-horizons

Highly crystalline covalent organic frameworks (COFs) or conjugated polymers (CPs) are very important and highly desirable because these materials would display better performance in diverse devices and provide more structure–property related information. However, how to achieve highly crystalline or single-crystal COFs and CPs is very challenging. Recently, many research studies have demonstrated the possibility of enhancing the crystallinity of COFs and CPs. Thus, it is timely to offer an overview of the important progress in improving the crystallinity of COFs and CPs from the viewpoint of design strategies. These strategies include polycondensation reaction optimization, improving the planarity, fluorine substitution, side chain engineering, and so on. Furthermore, the challenges and perspectives are also discussed to promote the realization of highly crystalline or single-crystal COFs and CPs.

1. Introduction

Covalent organic frameworks (COFs) and linear conjugated polymers (CPs) have attracted extensive attention in the fields of science and technology since their discovery.[1–7] Both COFs and CPs are made from light elements such as C, H, O, N, and S through covalent bonds. COFs are a class of porous polymers with two-dimensional (2D) or three-dimensional (3D) networks, while CPs are one family of one-dimensional (1D) semiconducting polymers whose repeated units are linked by sp^2 hybridized atoms.[8–11] Both COFs and CPs have several important advantages including light weight, high structure stability, and good chemical tunability.[12–24] To date, hundreds of COFs and CPs have been explored based on different organic building blocks such as benzene, pyridine, thiophene, acene, and natural dye molecules.[25–36] The good chemical tunability of COFs and CPs endows them with wide-ranging applications in energy storage and optoelectronic devices such as rechargeable batteries,[37–48] sensors,[49–52] organic field-effect transistors (OFETs),[53–57] organic light-emitting diodes (OLEDs),[58–61] and organic photovoltaics (OPVs).[49,62,63]

Crystallinity of COFs and CPs indicates the degree of long-range ordered periodic structure of atom arrangement in these materials, and thus it is one of the crucial features to determine

[a] *Department of Materials Science and Engineering, City University of Hong Kong, Hong Kong, SAR 999077, P. R. China. E-mail: qiczhang@cityu.edu.hk*
[b] *Center of Super-Diamond and Advanced Films (COSDAF), City University of Hong Kong, Hong Kong, SAR 999077, P. R. China*
† These authors contribute equally.

Jie Yang

Jie Yang received his BS and PhD degrees from the School of Chemistry and Chemical Engineering, Huazhong University of Science and Technology in 2014 and 2019, respectively. He is now working as a postdoctoral fellow in Prof. Qichun Zhang's group, City University of Hong Kong. His research interests include the synthesis and applications of novel covalent organic frameworks and conjugated polymers.

Fangyuan Kang

Fangyuan Kang received his Master's degree from Chengdu Institute of Organic Chemistry, Chinese Academy of Sciences in 2015. He is a PhD candidate in Prof. Qichun Zhang's group, City University of Hong Kong. His research interests include the design, synthesis, and applications of carbon-rich nanomaterials and crystalline covalent organic networks.

the properties and performance of COFs and CPs in diverse devices.[64–66] For example, high crystallinity (even single crystals) of COFs not only is favorable for their structural determination with lots of solid structural parameters including the pore size, atomic positions, and bond lengths and angles, but also significantly improves their performance in photocatalysis, proton conduction, energy storage, electronics, and other fields.[64] As to CPs, high crystallinity would offer rapid charge carrier (hole or electron) transport pathways through π–π stacking, which is very important to realize high-performance electronic applications such as OFETs, sensors, and logic circuits.[66] In particular, single-crystal CPs can offer a perfect platform to study the structure–property relationship and investigate the charge transport mechanisms in polymer systems. However, it still remains a big challenge to obtain highly crystalline or single-crystal COFs and CPs owing to the less reversibility or irreversibility of their covalent bond formation compared with the coordination bond and hydrogen bond formation in metal–organic frameworks (MOFs) and hydrogen-bonded organic frameworks (HOFs).[67–72]

Recently, lots of efforts have been made to achieve highly crystalline COFs and CPs. Strategies for achieving highly-crystalline or single-crystal COFs and CPs can be divided into two main categories: the optimization of polymerization reactions and the enhancement of the intramolecular or intermolecular interactions. For instance, Ma *et al.* developed a method to grow micrometer scale single-crystal COFs by adding a modulator.[64] The added modulator slowed down the rate of imine exchange and enhanced the reversibility of imine bond formation, offering enough time for the growth of COF single crystals. In this review, we will first provide a general introduction of COF and CP materials. Next, we will describe the strategies for improving the crystallinity of COFs and CPs. For COFs, the strategies include polycondensation reaction optimization, improving the planarity, hydrogen bond and fluorine substitution, and so on. For CPs, the strategies include thermal annealing, molecular mass modulation, improving the planarity, molecular geometry modulation, side chain engineering, fluorine substitution, and so on. This review will summarize the mechanisms of the crystallinity enhancement for each design strategy. The effect of crystallinity enhancement on practical applications will also be discussed. Finally, the conclusion and outlook of these strategies are provided.

2. Synthesis and comparison of COFs and CPs

COFs and CPs have several similar and different features. The similar features include the following: (1) both COFs and CPs are light-weight materials because they only contain light elements such as C, H, O, N, and S; (2) compared with MOFs and HOFs, COFs and CPs display high chemical stability since COFs and CPs are constructed through strong covalent bonds; (3) the properties of COFs and CPs can be tuned through the selection or modification of building blocks (Fig. 1 and 2), where these units can be benzene, pyridine, thiophene, acene, triazine, diketopyrrolopyrrole (DPP),[73–76] isoindigo,[77–80] naphthalene diimide (NDI),[81–83] and so on.[84,85] However, the different features between COFs and CPs are also obvious: (1) generally, the polymerization reactions of COFs are reversible, while those of CPs are not; (2) COFs have 2D or 3D porous structures, while CPs are 1D materials with negligible surface areas; (3) in most cases, CPs are solution-processable due to their bulky side chains, which can be processed through spin coating or printing technologies, while most of the COFs are insoluble in organic solvents.[56,86]

Since both COFs and CPs have wide applications in energy storage and optoelectronic devices such as LIBs, sensors, OFETs, OLEDs, and OPVs, developing different methods for their preparation is very important and highly desirable. Fig. 3 shows various synthetic methods to synthesize COFs and CPs. Most of the COFs are synthesized *via* reversible condensation reactions such as boronated ester formation, boronic acid trimerization, and Schiff base reactions (Fig. 3a).[87–92] The reversible nature of condensation reactions offers COF materials with a self-correction ability that can repair the structural defects, which permits the formation of crystalline COFs. In contrast, most CPs are obtained *via* irreversible polymerization reactions such as Stille, Suzuki, and direct arylation reactions (Fig. 3b).[93–99] Since these synthetic methods have been

Xiang Wang

Xiang Wang received his Master's degree from the School of Chemistry and Material Science, Nanjing Normal University in 2019. He is a PhD candidate in Prof. Qichun Zhang's group, City University of Hong Kong. His research focuses on developing novel methods for the fabrication of two-dimensional covalent organic frameworks and their single crystals.

Qichun Zhang

Qichun Zhang is a full professor at the Department of Materials Science and Engineering at City University of Hong Kong, China. His research focuses on carbon-rich conjugated materials and applications.

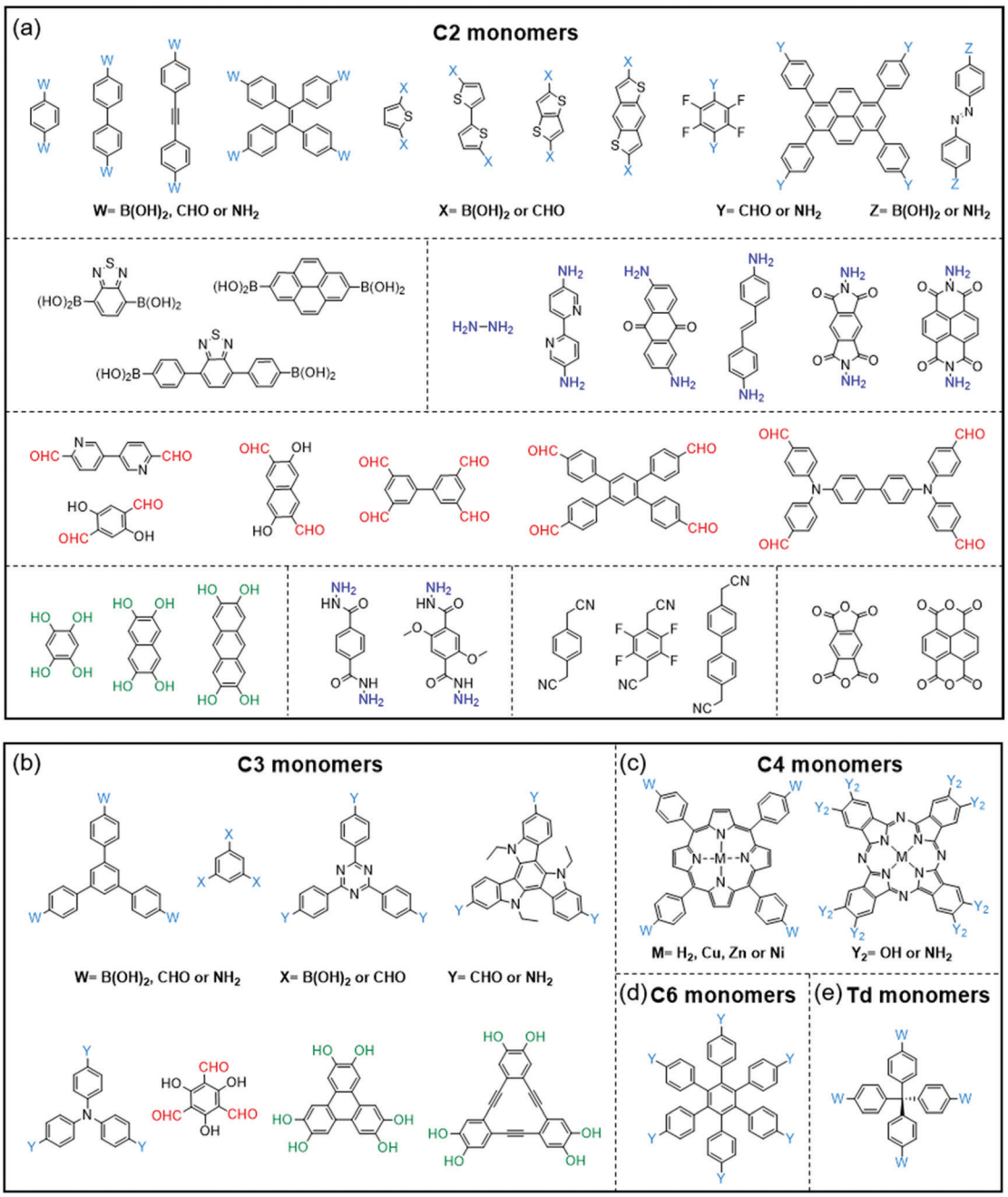

Fig. 1 Monomers with different geometries and reactive groups for the synthesis of COFs. The monomers can be divided into (a) C2, (b) C3, (c) C4, (d) C6 or (e) Td geometry.

summarized in several reviews,[10,12–14] here, we only focus on the strategies to improve the crystallinity of COFs and CPs during synthesis or processing.

3. Strategies for improving the crystallinity of COFs

Strategies for improving the crystallinity of COFs can be divided into several categories: polycondensation reaction optimization, improving the planarity, hydrogen bond and fluorine substitution, and so on. The advances of single-crystal COFs are also described.

3.1. Polycondensation reaction optimization

Polycondensation conditions of COFs are one of the common factors that can affect the crystallinity. The reaction conditions include catalyzed acids or bases, adding a modulator, the feeding rate of monomers, and so on. For example, highly crystalline COFs can be obtained by slowly adding the monomers because this operation can slow down the nucleation and crystal growth rates.[100,101] In fact, lots of studies have reported

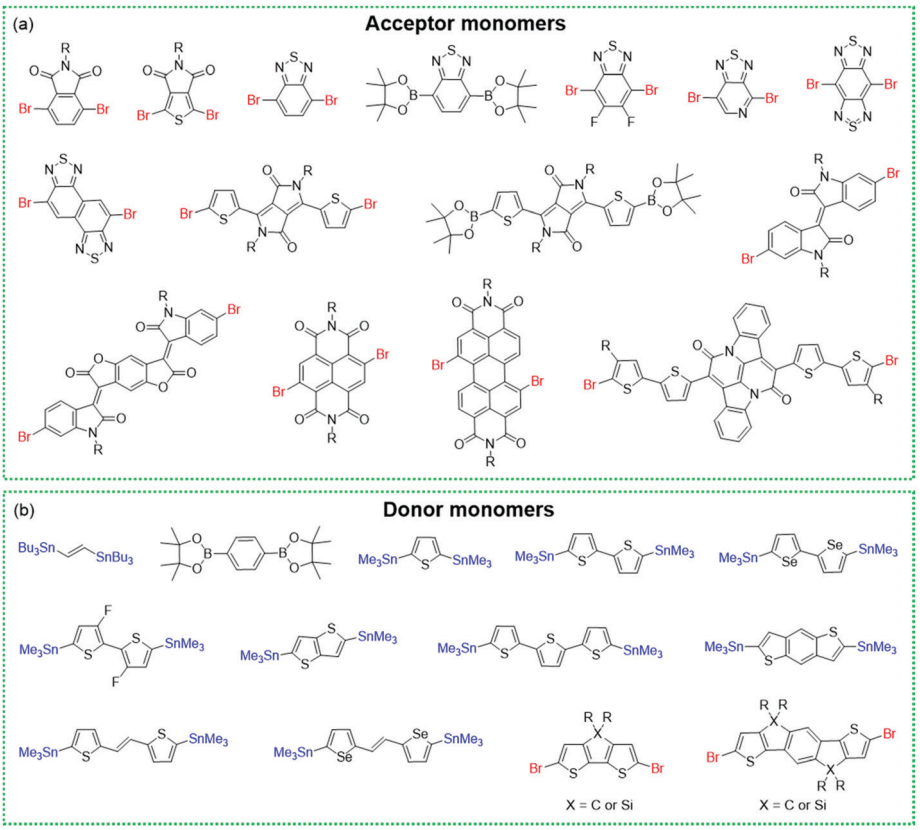

Fig. 2 (a) Selected acceptor or (b) donor monomers for the synthesis of CPs.

the effect of polycondensation conditions on the crystallinity of COFs. Here, we described several representative studies on polycondensation reaction optimization. Fig. 4 shows the representative examples of polycondensation reaction optimization to improve the crystallinity.

3.1.1 Acid catalyst. The crystallinity of COFs can be influenced by the types of acid catalysts in the polycondensation process. Matsumoto *et al.* replaced the traditional acetic acid catalyst with Lewis acidic metal triflates to synthesize a TAPB–PDA COF (Fig. 4a).[77] In contrast to the traditional acid-catalyzed methods that needed a high temperature and a long reaction time, metal triflates enhanced the rate of imine formation and exchange, providing highly crystalline COFs in several minutes at room temperature. Various metal triflates such as $Zn(OTf)_2$, $Y(OTf)_3$, $Yb(OTf)_3$, $In(OTf)_3$, $Eu(OTf)_3$, and $Sc(OTf)_3$ have been tried in the COF synthesis, where the COFs prepared in the presence of $Sc(OTf)_3$ displayed the strongest diffraction peaks. Focusing on $Sc(OTf)_3$ as the reaction catalyst and increasing its content from 0.002 to 0.02 equivalents, the authors found that the crystallinity of the as-obtained TAPB–PDA COFs gradually improved. To demonstrate the generality of this method, two new COFs (TAPB–BPDA COF and TAPB–TIDA COF) were also prepared with good crystallinity. Karak *et al.* believed that the hydrogen-bonding (H-bonding) strength would have a significant influence on the crystallinity of COFs, where its strength could be valued by the average H-bonding distance (d_{av}). To test this idea, they synthesized a series of acid-diamine salts by mixing selected acids (having various acid dissociation constants (K_a)) with different diamines, and then transformed the salts into corresponding COFs because H-bonding (N_{amine}–H···O_{acid}) interactions were easy to be found in the crystal structures of the acid-diamine salts.[102] The authors demonstrated that appropriate H-bonding strengths were essential to obtain highly crystalline COFs since strong hydrogen bonds within the diamine-acid salts would hinder the imine formation due to the lower reactivity with the aldehydes, while weak hydrogen bonds would result in faster reactions to form less ordered structures. They synthesized 49 COFs and concluded that the best d_{av} values were in the range of 2.06–2.19 Å. For example, when the diamine Pa-2 was crystallized with phenolsulfonic acid (PSA), *p*-toluenesulfonic acid (PTSA), benzenesulfonic acid (BSA), and 4-nitrobenzenesulfonic acid (NBSA), it displayed d_{av} values of 2.119, 1.875, 1.869, and 1.974 Å, respectively. The d_{av} value of the PSA-Pa-2 salt was within the range of 2.06 to 2.19 Å, which resulted in the TpPa-2 COF with the best crystallinity as compared with other salts.

3.1.2 Base catalyst. The strength of the bases also has a remarkable effect on the crystallinity of COFs. For example, Zhang *et al.* synthesized a series of covalent triazine frameworks (CTFs) (CTF-HUST-A1-K_2CO_3, CTF-HUST-A1-KOH, CTF-HUST-A1-EtOK, and CTF-HUST-A1-^{t}BuOK) by condensation reactions of benzylamine and amidine monomers using different bases.[103] The diffraction peak intensity in powder X-ray diffraction (PXRD) spectra became stronger with the increased strength of the bases. Among these CTFs, CTF-HUST-A1-^{t}BuOK achieved the

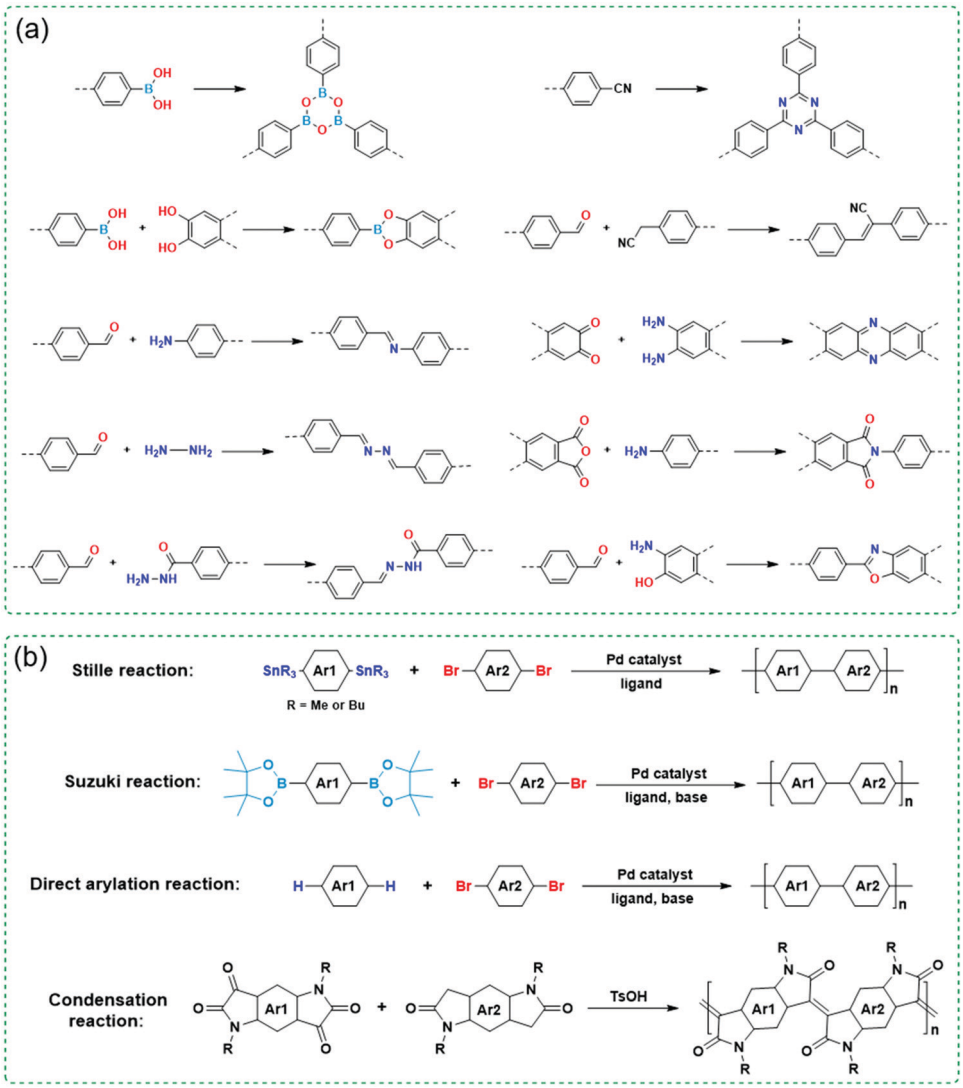

Fig. 3 Polymerization reactions for the synthesis of (a) COFs and (b) CPs. Ar represents aryl units and R represents side chains.

highest crystallinity and the Brunauer–Emmett–Teller (BET) surface areas also showed a similar tendency with CTF-HUST-A1-^{t}BuOK displaying the largest value of 644 m^2 g^{-1}. The CTFs were applied in photocatalytic water splitting and the hydrogen evolution rates (HERs) dramatically increased with the increase in crystallinity. CTF-HUST-A1-^{t}BuOK achieved the highest activity of 9200 μmol g^{-1} h^{-1}, which was about four times that of CTF-HUST-A1-K_2CO_3. Time-resolved transient absorption spectroscopy indicated that the crystalline structures could decrease the recombination of photogenerated charge carriers, thus improving the HERs.

3.1.3 Adding a modulator. Introducing a modulator into the polycondensation reaction can also improve the crystallinity of COFs. During the polycondensation process, the modulator can compete with the monomer and thus slow down the formation rates of COFs, which will offer enough time for self-correction of defects. Calik *et al.* designed a modulation approach for the growth of highly crystalline COF-5-*x*, where *x* represents the modulator content.[104] 4-Mercaptophenylboronic acid (MPBA) was selected as a modulator because its structure and solubility were similar to those of benzene-1,4-diboronic acid (BDBA). PXRD spectra indicated that the introduction of small amounts of MPBA resulted in enhanced crystallinity of the obtained COFs, as evidenced by sharper diffraction peaks. Compared with COF-5-0, COF-5-5 and COF-5-10 displayed several higher order diffraction peaks with stronger intensities, suggesting the presence of larger crystalline domain sizes and lower defect concentrations. The domain sizes increased with the increase of MPBA content up to x = 10 and then gradually decreased as the MPBA content was increased beyond 10%. COF-5-0 synthesized without MPBA showed a surface area of 1200 m^2 g^{-1}, while COF-5-10 obtained with 10% MPBA reached a larger surface area of 2100 m^2 g^{-1}. Transmission electron microscopy (TEM) images showed that the crystalline domain sizes increased from 30–50 nm (COF-5-0) to hundreds of nanometers (COF-5-10). Time-dependent PXRD indicated that the addition of modulators slowed down the rate of COF growth and promoted the self-healing of crystal defects. Another modulator (carboxyphenyl boronic acid

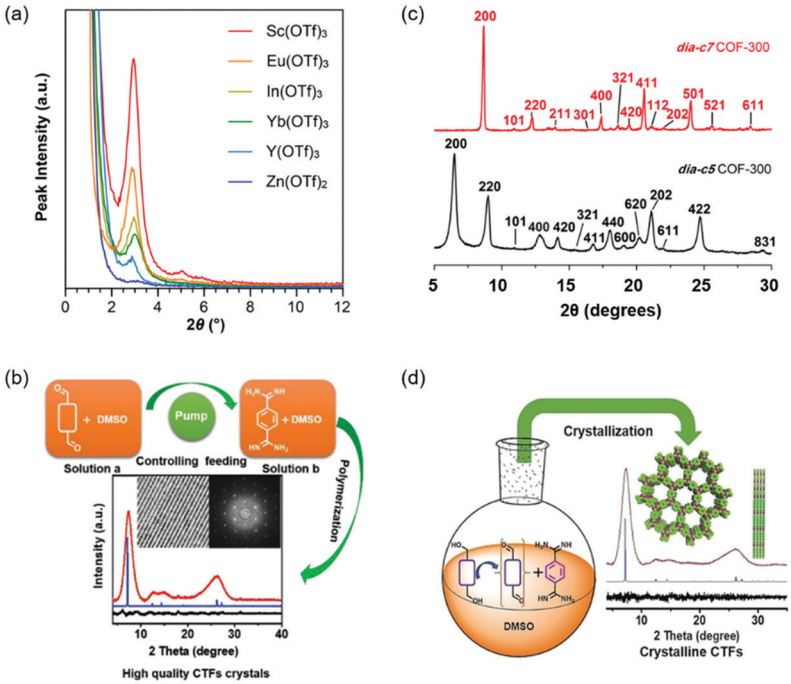

Fig. 4 Polycondensation reaction optimization of COFs. (a) PXRD patterns of the TAPB–PDA COF prepared using different metal triflate catalysts. Reproduced with permission.[77] Copyright 2017, American Chemical Society. (b) The method of controlling the nucleation rate and crystal growth by decreasing feeding rates to obtain highly crystalline CTFs. Reproduced with permission.[101] Copyright 2019, Wiley-VCH. (c) Comparison of the PXRD patterns of dia-c5 and dia-c7 COF-300 interpenetration isomers. Reproduced with permission.[107] Copyright 2018, American Chemical Society. (d) The method of improving the crystallinity of CTFs through *in situ* formation of aldehydes by controlled oxidation of alcohols. Reproduced with permission.[108] Copyright 2018, Wiley-VCH.

(CPBA)) could also influence the crystallinity and porosity of the resulting COFs, demonstrating the generality of the modulation strategy. Zhu *et al.* used benzaldehyde as a modulator to improve the crystallinity of an imine-based COF (TAPB–PDA COF), where the amount of the added benzaldehyde ranged from 0 to 9 equivalents relative to the monomer (TAPB).[105] PXRD spectra indicated that the crystallinity increased with the increase of the amount of added benzaldehyde. The improved crystallinity of COFs could result in a more ordered structure and a larger surface area. The COFs synthesized without benzaldehyde gave a surface area of 1378 m^2 g^{-1}, while the COFs obtained with 9 equivalents of benzaldehyde achieved a larger surface area of 2480 m^2 g^{-1}. Time-dependent PXRD indicated that benzaldehyde decreased the rate of COF nucleation and growth and increased the formation of crystalline domains, thus producing more ordered and crystalline COFs. To demonstrate the generality of this method, another imine-based COF (TAPB–TFPA COF) was also synthesized in the presence of benzaldehyde. As expected, the crystallinity and surface area increased with the increase of benzaldehyde content.

3.1.4 Controlling the monomer feeding rate. The monomer feeding rate can influence the crystallinity of COFs. Liu *et al.* prepared a highly crystalline CTF (CTF-HUST-HC1) by controlling the monomer feeding rate (Fig. 4b).[101] For comparison, a sample (CTF-HUST-1) was also synthesized without controlling the feeding rate. PXRD and TEM indicated that CTF-HUST-HC1 exhibited a much higher crystallinity than CTF-HUST-1 because the nucleation process and crystal growth were well regulated by tuning the monomer feeding rate. The controlled feeding rates of aldehyde monomer were 10, 30, 90, 180, and 800 μL min^{-1}. As shown in PXRD patterns, the full width at half maxima (FWHM) gradually decreased with the decreased feeding rate, suggesting that the size of crystals became bigger. The highly crystalline CTF-HUST-HC1, amorphous CTF-HUST-1, and g-C_3N_4 were used in photocatalytic applications. CTF-HUST-HC1 achieved superior performance in the photocatalytic removal of NO than CTF-HUST-1 and g-C_3N_4 due to the better separation of photogenerated electron–hole pairs and better charge transfer. These results demonstrated that highly crystalline COFs were beneficial for photocatalytic applications.

3.1.5 Other reaction conditions. Other reaction conditions that can slow down the formation rates of COFs will also improve the crystallinity of COFs. In 2009, Uribe-Romo *et al.* employed a solvothermal condensation reaction to synthesize a 3D COF (COF-300), which showed a 5-fold interpenetrated diamond topology (dia-c5).[106] Recently, Ma *et al.* reported the 7-fold interpenetration isomer (dia-c7) of COF-300 by adding an aging process (Fig. 4c).[107] In detail, the reaction mixture was kept at room temperature for 3 days and then heated at 50 °C for 3 days before heating at 120 °C for another 3 days. PXRD indicated that the diffraction peaks of dia-c7 COF-300 were much sharper and narrower than those of dia-c5 COF-300. The results suggested that the aging process could improve the crystallinity of COFs. 3D rotation electron diffraction (RED) data indicated that the maximal crystal size of dia-c7 COF-300

was up to 500 nm. Mechanism studies indicated that the more stable diac7 COF-300 formed *via* a thermodynamic route, while the dia-c5 COF-300 formed *via* a kinetic route. The aging process at lower temperatures offered enough time for the thermodynamic equilibrium, which was beneficial for the formation of diac7 COF-300. Liu *et al.* developed a simple strategy to obtain a series of CTFs through an *in situ* oxidation of alcohols into corresponding aldehyde monomers by dimethyl sulfoxide (DMSO) in an open system (Fig. 4d).[108] The resulting CTF-HUST-C1 achieved more diffraction peaks with stronger intensities compared with the reported CTF-HUST-1. CTF-HUST-C1 was synthesized by a two-stage heating procedure with an initial low temperature of 100 °C and then a relatively high temperature of 180 °C. The higher crystallinity of CTF-HUST-C1 might be attributed to the decrease of the nucleation rate resulting from the controlled oxidation of alcohol into aldehyde monomers in the low temperature stage and then an acceleration of crystal growth in the high temperature stage. To demonstrate the generality of this strategy, CTF-HUST-C5 and CTF-HUST-C6 were successfully obtained with good crystallinity. CTF-HUST-C1 exhibited a much higher photocatalytic performance than the reported amorphous CTF-HUST-1 due to its enhanced crystallinity. The hydrogen evolution rate of CTF-HUST-C1 was 5100 μmol h^{-1} g^{-1}, which was about three times that of CTF-HUST-1.

The crystallinity of COFs can be influenced by many reaction conditions, such as catalyzed acids or bases, adding a modulator, the feeding rate of monomers, and adding an aging process. Among these reaction conditions, adding a modulator and slowly adding the monomers are effective methods to improve the crystallinity by slowing down the formation rates of COFs.[101,104] The replacement of the traditional acetic acid catalyst with Lewis acidic metal triflates offers an important approach to synthesize crystalline COFs at room temperature.[77,109] In general, the relationship between the polycondensation reaction conditions and the crystallinity is complicated. It is highly desirable to explore other general and facile polycondensation methods for highly crystalline COFs.

3.2. Improving the planarity

Backbone planarity of 2D COFs is an important factor that can influence the crystallinity. Good backbone planarity of 2D COFs can promote interlayer π–π stacking of COF units, thus improving the crystallinity. Some monomers containing twisted groups may disrupt the interlayer π-stacking interactions and finally form amorphous porous polymers. The approaches to improve the planarity include introducing nitrogen atoms, removing twisted groups, and so on. For example, the replacement of C–H units in phenyl rings with nitrogen atoms can decrease the steric hindrance, resulting in an enhanced planarity.[110] Fig. 5 shows the crystallinity enhancement by planarity modulation.

Vyas *et al.* synthesized a series of 2D azine-linked COFs denoted as N_x-COF (x = 0, 1, 2, 3) based on the triphenylarene units with the central aryl moiety containing 0–3 nitrogen atoms (Fig. 5a).[110] As the number of nitrogen atoms was increased from zero to three, the planarity of N_x-COF gradually became better. For example, the dihedral angles between the central aryl and peripheral phenyl rings were 38.7° for N_0-COF and 0° for N_3-COF. The improvement of planarity was beneficial for higher crystallinity. PXRD indicated that the diffraction peak intensity of N_x-COF gradually increased with the increase of the content of nitrogen atoms (Fig. 5b). In addition, some crystalline domains with sizes of 50–100 nm could be observed in N_3-COF by TEM analysis. However, N_0-COF and N_1-COF did not display any crystalline domains. The N_x-COFs were used as photocatalysts in photocatalytic water splitting. The hydrogen evolution gradually increased from N_0-COF to N_3-COF, which was consistent with the enhanced crystallinity. Thompson *et al.* synthesized one COF (FLT-COF-1) and two covalent organic polymers (FLT-COP-2 and FLT-COP-3) based on fluoranthene units with different substitutions around the periphery.[111] Molecular dynamics (MD) simulations showed that the torsion angles around fluoranthene cores were increased as the attachment of more substituted phenyl groups. The extra steric hindrance of the attached phenyl rings led to poor planarity. As a result, the BET surface area of FLT-COF-1 was 1180 m^2 g^{-1}, which was about two times that of FLT-COP-2 or FLT-COP-3. Moreover, FLT-COF-1 was a mesoporous material, while FLT-COP-2 and FLT-COP-3 were microporous materials. PXRD indicated that FLT-COF-1 showed intense diffraction peaks with an eclipsed conformation. However, FLT-COP-2 and FLT-COP-3 were amorphous without obvious diffraction peaks. Xie *et al.* developed a hetero-porous COF (DBC-2P) based on dibenzo[*g*,*p*]chrysene units (Fig. 5c).[112] For comparison, a similar COF (4PE-2P) with tetraphenylethene (4PE) units as the knots was also prepared.[113] DBC units had a better planar backbone than 4PE units because the surrounding four phenyl rings were strictly fixed on the core by additional C–C single bonds. Compared with 4PE-2P, DBC-2P achieved enhanced crystallinity with much higher order and stronger diffraction peaks. DBC-2P showed stronger interlayer interactions than 4PE-2P due to the larger conjugated structure and better backbone planarity. The interlayer distance of DBC-2P (0.36 nm) was much shorter than that of 4PE-2P (0.45 nm). As a result, the crystallinity of DBC-2P was maintained after treatment with HCl, NaOH or boiling water. In contrast, the crystallinity of 4PE-2P disappeared after treatment with the above reagents. Based on the ordered 1D dual-pore nanochannels with high stability and crystallinity of DBC-2P, they prepared a hybrid material by incorporating linear polyethylene glycol (PEG) and PEG-$LiBF_4$ salt into the nanochannels and achieved a high ionic conductivity of 2.31×10^{-3} S cm^{-1}.

Improving the planarity of 2D COFs is an effective strategy to obtain crystalline COFs by promoting the π–π stacking of COF layers. The planarity can be improved by introducing sp^2-N atoms, avoiding twisted groups, or synthesizing large π-conjugated monomers. In particular, the introduction of sp^2-N atoms has been demonstrated as a general method to improve the planarity of aromatic molecules.[20] Except for the above approaches, more effective strategies to improve the planarity should be developed in the future.

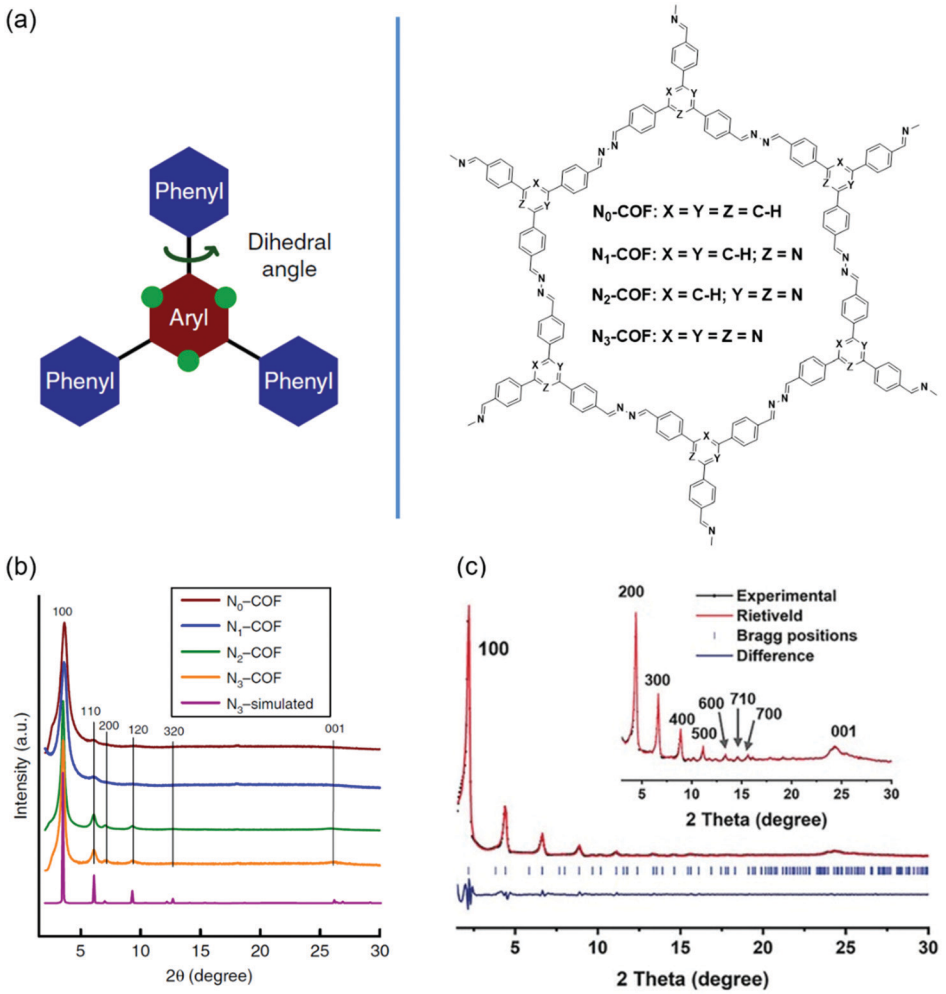

Fig. 5 Improving the crystallinity of COFs by planarity modulation. (a) Design and molecular structures of N_x-COFs with tunable N atoms. Reproduced with permission.[110] Copyright 2015, Springer Nature. (b) Experimental PXRD patterns of N_x-COFs. Reproduced with permission.[110] Copyright 2015, Springer Nature. (c) Experimental PXRD patterns (black dots) of DBC-2P. Reproduced with permission.[112] Copyright 2019, Wiley-VCH.

3.3. Hydrogen bond and fluorine substitution

The introduction of hydrogen bonds or fluorine atoms into 2D COFs has been demonstrated as an effective approach to improve their crystallinity.[114] The intralayer hydrogen bonds in 2D COFs can lock the molecular structure, improve the planarity of the 2D layers and thus enhance the crystallinity. Besides, the introduction of fluorine atoms can enhance interlayer π–π interactions based on self-complementary π-electronic forces, which will also improve the crystallinity.[115]

Hydrogen bonds can be divided into intralayer hydrogen bonds and interlayer hydrogen bonds. Fig. 6a and b show the examples of the intralayer hydrogen bond strategy to improve the crystallinity. Kandambeth *et al.* synthesized a 2D porphyrin COF (DhaTph) containing –OH units, which could form intramolecular O–H···N═C hydrogen bonds with adjacent C═N groups.[116] For comparison, a methoxy-substituted COF (DmaTph) without hydrogen bonds was also prepared. XRD data indicated that DhaTph showed a much more enhanced crystallinity compared with DmaTph. The intramolecular O–H···N═C hydrogen bonds in DhaTph could hold the phenyl units in one plane and enhance the structural rigidity, thus improving the crystallinity. However, the planarity between the phenyl units in DmaTph was lost, which was unfavorable for the 2D layer stackings and thus reduced the crystallinity. The surface area of DhaTph was much larger than that of DmaTph, which resulted from the improved crystallinity. In addition, DhaTph retained its crystallinity in HCl and boiling water, while DmaTph was unstable in these conditions. Chen *et al.* elucidated the effect of intramolecular H-bonding interactions on the crystallinity, porosity, and photochemical activity of 2D COFs by three-component condensation reactions to synthesize a series of 2D porphyrin COFs (named MP-DHPh$_X$ COFs when X = 25, 50, 75 and where M = H_2, Cu, and Ni; and MP-DHPh COFs when X = 100 and where M = H_2, Cu, and Ni), in which intramolecular H-bonding sites were tunable (Fig. 6a).[117] For comparison, amorphous porphyrin polymers (named MP-Ph polymers when X = 0) were also prepared. XRD patterns showed that the crystallinity of MP-DHPh$_X$ COFs was much higher than that of the amorphous MP-Ph polymer without H-bonding interactions. The diffraction peak intensity

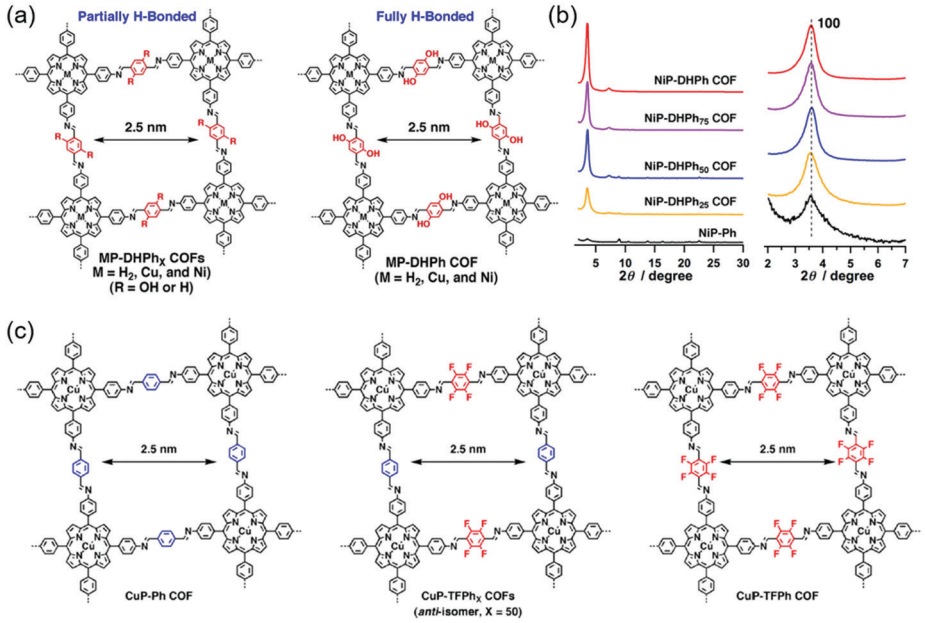

Fig. 6 Improving the crystallinity of COFs by hydrogen bond and fluorine substitution. (a) The molecular structures of 2D COFs with tunable content of hydrogen bonds. Reproduced with permission.[117] Copyright 2015, American Chemical Society. (b) XRD patterns of the NiP-DHPh$_X$ COFs. Reproduced with permission.[117] Copyright 2015, American Chemical Society. (c) The molecular structures of 2D COFs with tunable content of F atoms. Reproduced with permission.[115] Copyright 2013, American Chemical Society.

of MP-DHPh$_X$ COFs gradually increased with the increase of the content of dihydroxyterephthalaldehyde (DHTA) (Fig. 6b). Theoretical calculations indicated that the dihedral angles between the imine linkage and *meso*-phenyl units of porphyrin in MP-DHPh$_X$ were quite smaller than those of MP-Ph polymers, where the total crystal stacking energy in these materials was opposite. Therefore, the amorphous MP-Ph polymer displayed inferior planarity and needed more energy to form crystalline frameworks, indicating that the H-bonding interactions improved the π-stacking interactions and enhanced the crystallinity by promoting the planar conformation. These COFs were applied in photocatalytic conversion reactions of molecular oxygen into singlet oxygen. The photocatalytic activity of MP-DHPh$_X$ gradually increased with the increase of the content of H-bonding sites, which was consistent with the crystallinity tendency. Guo *et al.* synthesized a series of 2D COFs, namely TPT–BD COF, TPT–DHBD$_X$ COFs (X = 25, 50, and 75 mol%), and TPT–DHBD COF.[118] These COFs were composed of benzidine (BD) and 3,3′-dihydroxybenzidine (DHBD) units with molar ratios of 0/100, 25/75, 50/50, 75/25, and 100/0. PXRD patterns indicated that all the COFs showed (100), (110), (200), (210), and (220) diffraction peaks. The diffraction peak intensities of the TPT–BD COF, TPT-DHBD$_X$ COFs, and TPT–DHBD COF gradually increased with the increase of the content of DHBD. The enhanced crystallinity of the COFs was attributed to the formation of intramolecular hydrogen bonds between the phenolic hydroxyl group and the imine–nitrogen atom through a five-membered ring. The additional H-bonding interactions locked the partial structure of the COFs, which improved the planarity of the 2D layers and thus enhanced the crystallinity.

The introduction of interlayer hydrogen bonds can also improve the crystallinity of COFs. Halder *et al.* developed a COF (TpOMe-Pa1) based on 2,4,6-trimethoxy-1,3,5-benzenetricarbaldehyde (TpOMe) *via* a *p*-toluenesulfonic acid (PTSA) mediated solid-state mixing approach.[119] For comparison, a similar polymer (Tf-Pa1) based on 1,3,5-benzenetricarbaldehyde (Tf) was also prepared. PXRD indicated that TpOMe-Pa1 showed high crystallinity with clear (100), (110), (210), and (001) diffraction peaks. In contrast, Tf-Pa1 was an amorphous polymer. The BET surface area of TpOMe-Pa1 was 1164 $m^2\ g^{-1}$, which was much higher than that of Tf-Pa1. Moreover, TpOMe-Pa1 displayed high chemical stability in extreme conditions such as strong acids and bases. Theoretical calculations indicated that a number of interlayer C–H···N hydrogen bonds between the methoxy C–H units of a particular layer and the imine N atoms of the adjacent layers formed in TpOMe-Pa1. The presence of interlayer hydrogen bonds in TpOMe-Pa1 improved the crystallinity and chemical stability.

Fig. 6c shows the examples of fluorine substitution to improve the crystallinity. Chen *et al.* proposed a strategy to improve the crystallinity of COFs by controlling the interlayer interactions based on self-complementary π-electronic forces.[115] To demonstrate the strategy, they synthesized a series of COFs, namely CuP–Ph COF, CuP–TFPh$_X$ COFs (X = 25, 50, and 75 mol%), and CuP–TFPh COF (Fig. 6c). These COFs were composed of tetrafluorophenyl (TFPh) and phenyl (Ph) units with molar ratios of 0/100, 25/75, 50/50, 75/25, and 100/0. XRD patterns showed clear (100), (200), and (001) diffraction peaks, indicating that all the COFs displayed good crystallinity. The XRD intensity gradually increased from the CuP–Ph COF to the CuP–TFPh$_{50}$ COF. Further increase in the content of TFPh led to the decrease in the XRD intensity. Among all the

COFs, the CuP–TFPh$_{50}$ COF exhibited the strongest XRD intensity. The BET surface areas of the COFs also displayed a similar tendency with CuP–TFPh$_{50}$ COF showing the largest value of 1389 m^2 g^{-1}. Theoretical calculations revealed that the interlayer π–π interactions between fluoro-substituted and non-substituted arenes increased the total crystal stacking energy of the COFs, thus resulting in high crystallinity. All the results elucidated that the self-complementary π-electronic interactions could improve the crystallinity of COFs. Alahakoon *et al.* synthesized two COFs (TF-COF 1 and TF-COF 2) containing fluorine atoms.[120] For comparison, a non-fluorinated COF (NF-COF) was also prepared. PXRD patterns showed that the (100), (110), (120), (130), and (001) diffraction peaks could be clearly observed in TF-COF 1 and TF-COF 2, indicating their good crystallinity. However, only two diffraction peaks at 3.67° and 6.09° were observed for the NF-COF, suggesting a lower degree of crystalline order. The BET surface areas of TF-COF 1 and TF-COF 2 were 1820 and 2044 m^2 g^{-1}, respectively, which were much higher than that of the NF-COF. Moreover, TF-COF 1 and TF-COF 2 showed more well-defined pore structures compared with the NF-COF. All the results demonstrated that the rational introduction of fluorine atoms into the COF structures could significantly improve the crystallinity.

The crystallinity of COFs can be improved by introducing hydrogen bonds or fluorine atoms. Both hydrogen bond and fluorine substitution can enhance the π-stacking interactions of COFs, which will promote the COF crystallization. Besides, hydrogen bonds can enhance the planar conformations of COFs, which will further improve the crystallinity. However, the studies of hydrogen bond and fluorine substitution mainly focus on 2D COFs.[115,116] The effect of hydrogen bond and fluorine substitution on the crystallinity of 3D COFs needs further studies. In addition, other functional groups such as Cl, CN, and CF_3 can also be introduced into COFs to improve the crystallinity.

3.4. Other strategies

Other strategies to improve the crystallinity of COFs include a two-in-one strategy, a group protection approach, molecular symmetry or side chain modulation, and so on.[121–125] Fig. 7 lists some of them.

Recently, a two-in-one strategy and a group protection approach have been developed to improve the crystallinity of COFs.[121] Li *et al.* reported a two-in-one design strategy to synthesize 2D imine COFs in facile conditions. A bifunctional monomer with two aldehyde and amino groups in one pyrene unit was used to synthesize a 2D pyrene-based COF (Py-COF) through self-condensation.[121] The stoichiometry of the aldehyde and amino groups in the monomer was strictly guaranteed (1 : 1), which was favorable for the formation of crystalline COFs. A series of highly crystalline Py-COFs were achieved not only in mixed organic solvents but also in single solvents such as methanol, acetonitrile, dichloromethane, and tetrahydrofuran. For comparison, the reported Py–Py COF, which had a similar molecular structure to the Py-COF, was prepared by the traditional co-condensation reaction.[126] The crystallinity of the Py-COF was better than that of the Py–Py COF, as revealed by the PXRD results. Moreover, the Py–Py COFs obtained through a co-condensation method in a single solvent showed poor crystallinity. The two-in-one strategy was also used to grow crystalline Py-COF films on

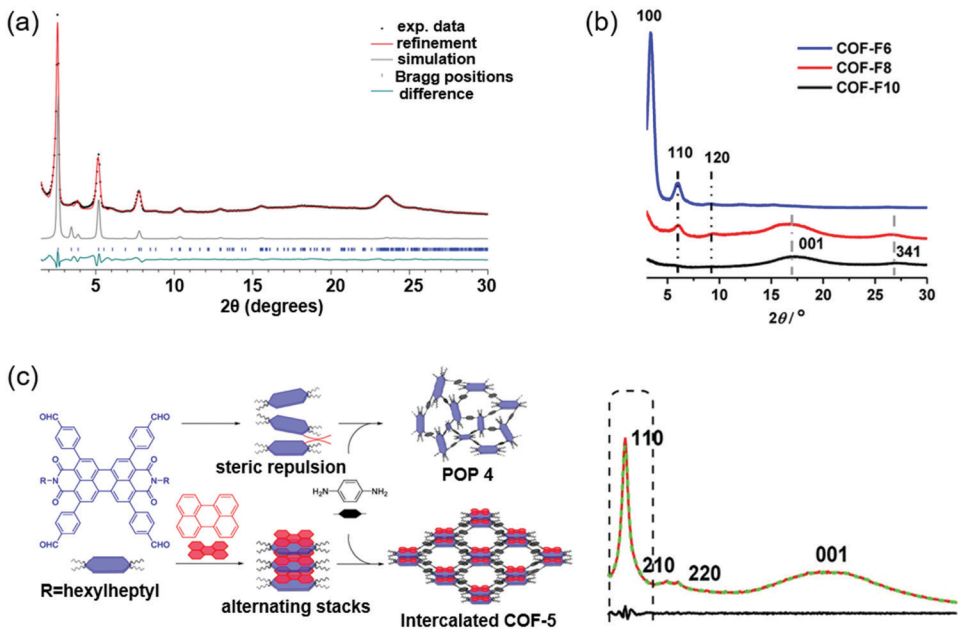

Fig. 7 Improving the crystallinity of COFs by other strategies. (a) Experimental PXRD data (black dots) of Py–a4T COF. Reproduced with permission.[123] Copyright 2017, American Chemical Society. (b) PXRD data of COF-F_X. Reproduced with permission.[124] Copyright 2020, American Chemical Society. (c) Synthetic schematic of POP 4 in the absence and intercalated COF-5 in the presence of D–A interactions (left). PXRD data of intercalated COF-5 (right). Reproduced with permission.[130] Copyright 2020, American Chemical Society.

substrates such as glass and silicon wafer. Such COF films could be applied as charge-transport layers in perovskite solar cells. To demonstrate the generality of this method, another kind of dual-pore COFs (BFBAEB-COF and BFBAEPy-COF) were successfully prepared.[121,127] These COFs could not be synthesized by the traditional co-condensation approach. Chen *et al.* developed a "two-in-one" strategy to synthesize a bicarbazole-based COF (BCzP-COF) by a self-polycondensation reaction of the A_2B_2 monomer with two amine and two neopentyl acetal units.[128] The neopentyl acetal unit was an aldehyde protecting group. For comparison, another COF (BCz-COF) was also prepared by a reaction of the A_2B_2 monomer with free amines and aldehydes. PXRD indicated that both COFs showed (110), (220), (330), and (001) diffraction peaks. However, the diffraction peak intensity of the BCzP-COF was stronger than that of the BCz-COF. Scanning electron microscopy (SEM) patterns revealed that both COFs displayed rod-like microcrystals. The crystal length of the BCzP-COF was much longer (about 20 μm) than that of the BCz-COF. The BET surface area of the BCzP-COF was 2200 $m^2\ g^{-1}$, which was much higher than that of the BCz-COF. All these results demonstrated that the BCzP-COF achieved better crystallinity than the BCz-COF. Bai *et al.* synthesized a COF (PI-2-COF) through a condensation reaction between an aryl amine and an aldehyde.[129] The as-prepared COF showed moderate crystallinity with a surface area of 1286 $m^2\ g^{-1}$. Later, Vitaku *et al.* synthesized a BND–TFB COF through a modulated condensation reaction between a benzophenone–imine protected monomer and an aldehyde.[122] PXRD diffraction peaks indicated that the BND–TFB COF showed an improved crystallinity compared with the PI-2-COF. The higher crystallinity was achieved by the controlled release of free amine groups *via* slow removal of the benzophenone imine protecting groups. As a result, the BND–TFB COF displayed a high surface area of 2618 $m^2\ g^{-1}$, which was much higher than that of the PI-2-COF. Moreover, the generality of this method was further demonstrated by the successful synthesis of other COFs including TAPB–PDA COF, DAB–TFP COF, and BND–TFP COF.

Molecular symmetry and side chains can have a remarkable effect on the crystallinity of COFs. Keller *et al.* prepared a symmetric unit and an asymmetric unit of the dibutyl-quaterthiophene (4T).[123] No crystalline COF could be formed based on the symmetric 4T and 1,3,6,8-tetrakis(4-aminophenyl)pyrene (Py). Cofacial stacking of the symmetric 4T unit could bring the alkyl chains of adjacent layers very close, causing obvious steric repulsion and impeding the formation of a crystalline COF. In contrast, a crystalline COF (Py–a4T COF) was formed based on the asymmetric 4T and Py because the steric repulsion could be avoided in the asymmetric 4T unit. PXRD indicated that the Py–a4T COF showed multiple higher-order diffraction peaks, which suggested the high degree of long-range order formed in the COF (Fig. 7a). The asymmetric functionalization strategy could also be used in other building blocks. For example, crystalline COFs could be obtained based on asymmetric 4*H*-thieno[3,4-*c*]pyrrole-4,6(5*H*)-dione (TPD) or thieno[3,4-*b*]thiophene (TT) units. Charge transfer states between the subunits of the COFs were observed, as revealed by the time-correlated single photon counting (TCSPC) traces. In another study, Wu *et al.* synthesized a series of perfluoroalkyl-functionalized 2D COFs (COF-F6, COF-F8, and COF-F10) and investigated the influence of different lengths of perfluoroalkyl chains on the crystallinity and proton conductivity.[124] PXRD indicated that COF-F6 showed multiple high-order diffraction peaks, suggesting the high crystallinity of COF-F6. The diffraction peak intensity gradually decreased from COF-F6 to COF-F10 because the longer perfluoroalkyl chains might cause steric repulsion and could be unfavorable for the crystallinity (Fig. 7b). The COFs displayed good chemical stability and hydrophobic properties due to the presence of perfluoroalkyl chains. These COFs could be used as hosts to load H_3PO_4 for proton conduction. The highest proton conductivity of COF-F6 was 4.2×10^{-2} S cm^{-1} after H_3PO_4 doping. In comparison, COF-F8 and COF-F10 displayed lower proton conductivities, which was due to the facts that (i) the longer perfluoroalkyl chains could block the proton transport pathway in the COFs, and (ii) the lower crystallinity further decreased the proton transport efficiency. Li *et al.* developed a donor–acceptor (D–A)-type intercalated COF by a supramolecular assembly strategy.[130] A solvothermal reaction between 2,5,8,11-tetra(*p*-formylphenyl)-perylene diimide (PDI) and *p*-phenylenediamine afforded an amorphous porous polymer. This was because the long alkyl chains of PDI could cause obvious steric repulsion, which hindered the interlayer stacking of COFs. However, if perylene was added before the solvothermal reaction, an intercalated COF was obtained. An associating D–A complex could form between the electron-deficient PDI and electron-rich perylene, which decreased the steric repulsion of the alkyl chains. As a result, an intercalated COF based on PDI and *p*-phenylenediamine could be synthesized (Fig. 7c). XRD indicated that the intercalated COF showed good crystallinity with AA-stacking.

Recently, other strategies including a two-in-one strategy, a group protection approach, and molecular symmetry or side chain modulation have been developed to improve the crystallinity of COFs. The two-in-one strategy can guarantee the precise stoichiometry of the monomers in the polycondensation reaction, which is beneficial for the formation of crystalline COFs.[121] In the group protection approach, a free amine or aldehyde monomer will be slowly released *via* the removal of the protecting groups, thus decreasing the reaction rate of the reversible imine formation and improving the crystallinity.[122] Molecular symmetry or side chain modulation can improve the crystallinity of COFs by decreasing the steric repulsion of side chains.[123,124] Despite the advances of the above strategies, their studies are still limited. These strategies can be applied in new COFs to improve the crystallinity.

3.5. Single-crystal COFs

The realization of single-crystal COFs is challenging but very important for several reasons: (1) the determination of COF structures from PXRD is extremely difficult, especially for the COFs with complicated topology structures; (2) single-crystal data can enable precise structural characterization of COFs such as the porous structure, atomic positions, and bond lengths and angles; (3) compared with polycrystalline COFs, single-crystal COFs generally display better performance in gas

absorption, photocatalysis, electronic devices, and so on.[64] The first single-crystal COF was achieved by Beaudoin *et al.* in 2013.[131] Recently, Evans *et al.* reported a single-crystal COF by a two-step seeded growth strategy.[100] Ma *et al.* developed a general method to grow micrometer scale single-crystal COFs by adding a modulator.[64] The effect of single-crystal size on the crystallinity, structural flexibility, and gas absorption properties was further investigated.[132] The key point to achieve single-crystal COFs is to modulate the reversible process during the linkage bond formation, offering enough time for self-correction of defects. Fig. 8 shows the reported single-crystal COFs.

Beaudoin *et al.* successfully synthesized high quality 3D COF crystals by reversible self-addition polymerizations, allowing the structures of these materials to be characterized by single-crystal XRD.[131] A series of single-crystal COFs, NPN-1, NPN-2, and NPN-3, were synthesized *via* oxidation polymerization of the nitroso compounds of tetrakis(4-nitrosophenyl)methane, tetrakis(4-nitrosophenyl)silane, and 1,3,5,7-tetrakis(4-nitrosophenyl) adamantane, respectively. The single crystals were large and uniform in morphology, with their size reaching 0.5 mm in the case of NPN-3. NPN-1 and NPN-2 were both observed to crystallize in the tetragonal space group $P\bar{4}$ and give diamondoid networks with four-fold interpenetration. NPN-3 was found to crystallize in the tetragonal space group $P4_2/n$ and showed a diamondoid network with six-fold interpenetration. Zhang *et al.* reported another single-crystal 3D COF (COF-320).[133] SEM revealed that COF-320 showed a uniform rice-like morphology with a crystal dimension of about 200 nm. The single-crystal structure of COF-320 was investigated by 3D RED for the first time. COF-320 had a highly porous diamond net with 9-fold interpenetration. The RED data indicated that COF-320 formed a body-centered orthorhombic crystal structure. COF-320 showed a large Langmuir surface area of 2400 $m^2\ g^{-1}$ due to the good crystallinity. As a result, COF-320 achieved a high methane uptake capacity of 15.0 wt% at 298 °C and 80 bar. Gao *et al.* designed three isostructural 3D COFs with –H, –Me, or –F substituents (3D-TPB-COF-H, 3D-TPB-COF-Me, and 3D-TPBCOF-F).[134] SEM indicated that these 3D-TPB-COFs had uniform morphology with a crystal dimension of about 1 μm. All 3D-TPB-COFs showed sharp and intense diffraction peaks, indicating a highly crystalline nature. Their crystal structures were investigated by RED with the resolution reaching up to 0.9–1.0 Å, elucidating the positions of all non-hydrogen atoms in COFs. All 3D-TPB-COFs showed the same five-fold interpenetrated topologies with the different substituents being visible. All 3D-TPB-COFs displayed different gas absorption properties, such as selectivity for CO_2 over N_2. 3D-TPBCOF-F with C–F bonds on the porous structure achieved the highest selectivity. In another study, Xu *et al.* reported a single-crystalline 1D metallo-COF (mCOF-Ag) by combining metal–ligand coordination and dynamic imine condensation (Fig. 8a).[135] mCOF-Ag was synthesized by a one-pot reaction between 4,4′-(1,10-phenanthroline-2,9-diyl)dianiline (I) and 2,9-bis(4-(dimethoxymethyl)phenyl)-1,10-phenanthroline (II) in the presence of $AgBF_4$. Monomer II with acetal groups showed good solubility and was favorable for the self-assembly process. Compared with amine groups, the acetal groups displayed lower reactivity, which could decrease the crystal nucleation rate to form good crystals. The coordination bonds between silver ions and phenanthroline units of I and II were beneficial for the crystal formation. SEM revealed that mCOF-Ag possessed a uniform rod-like morphology with crystal lengths exceeding 2 μm. The single-crystal nature of mCOF-Ag was confirmed by high-resolution TEM and selected-area electron diffraction (SAED). Single-crystal electron diffraction (SCED) indicated that mCOF-Ag

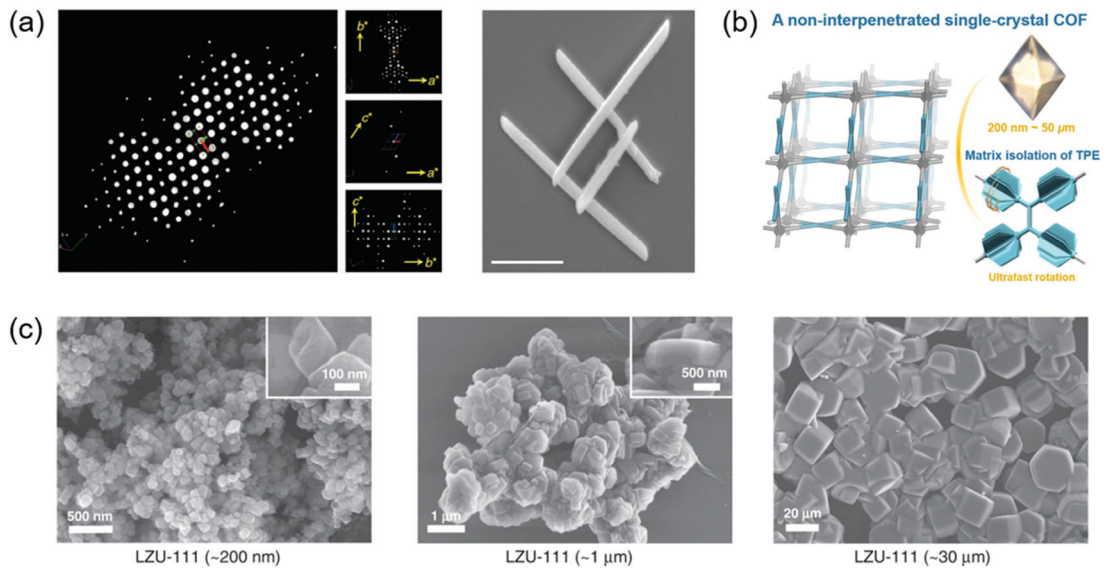

Fig. 8 Single crystals of COFs. (a) 3D reciprocal lattice of mCOF-Ag obtained from the SCED data and SEM image of mCOF-Ag. Scale bar: 1 μm. Reproduced with permission.[135] Copyright 2020, Springer Nature. (b) A single-crystal COF with non-interpenetrated pts topology. Reproduced with permission.[138] Copyright 2020, Wiley-VCH. (c) SEM images of different-sized LZU-111 crystals. Reproduced with permission.[132] Copyright 2020, Springer Nature.

showed a monoclinic crystal structure. Since mCOF-Ag had amine groups, it could react with glyoxal to give wCOF-Ag through crystalline-state polymerization. The crystal structure of wCOF-Ag was maintained, as established by PXRD.

Evans *et al.* developed a two-step seeded growth strategy to prepare a single-crystalline 2D COF (COF-5).[100] A stable colloidal COF-5 suspension was prepared in the first step.[136] Then single-crystalline COF-5 was formed in the second growth step, in which the monomers were introduced slowly into the solution. The monomer addition rates in the second step were crucial for the formation of COF single crystals. Dynamic light scattering (DLS) suggested that the COF-5 particle size increased from 400 nm to 1000 nm after 4.0 equiv. of 2,3,6,7,10,11-hexahydroxytriphenylene (HHTP) was added at a slow rate of 0.1 equiv. h^{-1}. Wide-angle X-ray scattering (WAXS) indicated that the diffraction peak intensity gradually increased with slow addition of the monomers. In contrast, when HHTP was added rapidly (1.0 equiv. h^{-1}), the average particle size gradually decreased. To demonstrate the generality of the seeded growth strategy, two other 2D COFs (COF-10 and TP-COF) were synthesized using this strategy. Single-crystalline COF-10 and TP-COF were also obtained when the monomers were added slowly. TEM characterization indicated that the maximum sizes of COF-5 and COF-10 could reach 1 and 5 μm, respectively. Later, Evans *et al.* developed a general strategy to synthesize a series of single-crystalline colloidal COFs (Ph-COF, BPh-COF, DBD-COF, Py-COF, and TMPh-COF) by introducing nitrile-containing cosolvents.[137] DLS measurements suggested that the Ph-COF particle size increased from 100 nm to 400 nm with the increase of monomer concentration from 5 mM to 15 mM. The crystallinity of the COFs was confirmed by synchrotron XRD. TEM suggested that the COFs showed crystal sizes of several hundred nanometers. Fast Fourier transform (FFT) indicated that all COF particles displayed crystalline spot patterns, suggesting the single-grain crystallinity. Solution fluorescence spectroscopy indicated that the COF suspensions were highly emissive compared with their boronic acid monomer solutions, which was attributed to the through-space electronic communication of chromophores between COF sheets. Ma *et al.* developed a general approach to grow large single crystals of 3D imine-linked COFs by using aniline as a modulator.[64] In the synthesis of a typical imine-linked COF, an amorphous solid firstly formed and then transformed into a crystalline phase *via* imine exchange conversion. It is a feasible approach to improve the crystallinity of the COF by decreasing the rate of imine exchange. Monofunctional aniline can act as a nucleation inhibitor to modulate the crystallization process because its reactivity is similar to that of the amino monomer. After the addition of aniline, the imine bond formation remained fast. The rate of imine exchange was slowed down, which provided enough time for the growth of COF single crystals. By using this method, a single crystal of COF-300 up to 100 μm was obtained. In addition, the crystal size of COF-300 was tunable by controlling the amount of aniline. To demonstrate the generality of this method, several single crystals of other 3D imine-linked COFs including COF-303, LZU-79, and LZU-111 were obtained. Based on the single-crystal XRD data of COF-300, its degree of interpenetration was confirmed, and the arrangement of water guests in hydrated COF-300 was determined. Liang *et al.* reported the first non-interpenetrated single-crystal COF (LZU-306) by employing the aniline-based modulation method (Fig. 8b).[138] The crystals with a size of 200 nm were synthesized under the traditional reaction conditions without aniline. In the presence of aniline, single crystals of LZU-306 were obtained. The single crystal size became larger with the increase of the amount of aniline. Single-crystal XRD indicated that LZU-306 showed a non-interpenetrated *pts* structure. PXRD of LZU-306 displayed sharp peaks with a very small FWHM due to the high quality of the crystals. LZU-306 exhibited a large BET surface area of 2059 $m^2 g^{-1}$ with an average pore width of 10.9 Å. With a highly open structure, LZU-306 was used to explore the intrinsic dynamics of the tetraphenylethylene (TPE) as the individual aggregation induced-emission (AIE) unit. Later, Ma *et al.* systematically studied the effect of the crystal size of COFs on their respective properties by synthesizing a series of LZU-111 and COF-300 with different crystal sizes (Fig. 8c).[132] Single-crystal LZU-111 and COF-300 with various crystal sizes (200 nm, 1 μm, and 30 μm for LZU-111; 500 nm, 1 μm, and 30 μm for COF-300) were prepared by adjusting the amount of modulator. For LZU-111, the FWHM of the diffraction peaks in the PXRD patterns of variable-sized crystals decreased with the increase of the crystal size from 200 nm to 30 μm, which indicated that the crystallinity of LZU-111 was enhanced from nanocrystal to micrometer crystals. For COF-300, the FWHM of the diffraction peaks of variable-sized crystals only slightly decreased with the increase of crystal size. The effect of crystal sizes on the gas sorption behaviors of the COFs was explored. The N_2 and Ar uptakes of LZU-111 increased with the increase of crystal size. However, the N_2 and Ar uptakes of COF-300 decreased with the increase of crystal size. This was because COF-300 had a flexible structure. Small crystals of COF-300 were more flexible and could be more easily stretched or compressed, which was favorable for N_2 and Ar uptakes. Large single crystals of COF-300 were more rigid and unfavorable for gas uptake.

Lots of efforts have been made to synthesize single-crystal COFs. Until now, only several single-crystal COFs have been reported based on several methods such as reversible self-addition polymerizations, adding a modulator, and a two-step seeded growth strategy.[64,100,131] In particular, a general method has been demonstrated to grow micrometer scale single-crystal COFs by adding a modulator.[64] The largest crystal size by this method can reach 100 μm. However, the reported single-crystal COFs are mainly based on the boronate ester formation and Schiff base reactions. Single-crystal COFs synthesized by other reactions remain to be explored. Moreover, it is challenging to synthesize 2D single-crystal COFs, which offer potential applications in organic electronics such as transistors and luminescent devices.

4. Strategies for improving the crystallinity of CPs

In general, CPs are prepared using irreversible coupling reactions. The main strategies for improving the crystallinity of CPs are

based on the mechanism of enhancing the intramolecular or intermolecular interactions. The strategies can be divided into several categories: thermal annealing, molecular mass modulation, improving the planarity, molecular geometry modulation, side chain engineering, fluorine substitution, and so on. The advances of conjugated polymer crystals are also discussed. Although crystalline CPs have wide applications in various optoelectronic devices, in this part, we focus only on their applications in OFETs.

4.1. Thermal annealing

Thermal annealing is a widely used approach to improve the crystallinity of CPs. Since CP films can achieve the best crystallinity at the optimal annealing temperature, the effect of thermal annealing on polymer crystallinity has been extensively studied. Here, we introduced several representative studies in this part. Fig. 9 shows some examples of thermal annealing to improve the crystallinity.

Sonar *et al.* developed a DPP-based polymer (PDPP-TBT).[139] The influence of thermal annealing on polymer crystallinity was systematically investigated. XRD characterization suggested that the as-spun polymer film was almost amorphous without diffraction peaks. When the films were subjected to thermal annealing, the diffraction peaks appeared and became sharper. The diffraction peak intensity became stronger with increasing annealing temperature. After annealing at 200 °C, the film displayed the strongest (100) and (010) diffraction peaks. Atomic force microscopy (AFM) phase images indicated that the annealed films became more ordered and formed interconnected networks between the nanofiber domains with increasing annealing temperature. As a result, OFETs based on PDPP-TBT showed higher mobilities as the annealing temperature was increased. The devices annealed at 200 °C achieved the highest hole and electron mobilities of 0.35 and 0.4 $cm^2 V^{-1} s^{-1}$, respectively. Ha *et al.* reported a DPP-based polymer (P(DPP-*alt*-DTBSe)).[140] XRD characterization indicated that the as-spun and annealed polymer films showed (*h*00) peaks up to fourth order. Annealing the films at 150 or 180 °C increased the intensity of the (*h*00) peaks, indicating the enhancement of the crystallinity. The film displayed the strongest (*h*00) peaks after annealing at 180 °C. OFETs based on P(DPP-*alt*-DTBSe) exhibited higher mobilities with increasing annealing temperature. The devices that were annealed at 180 °C achieved the highest hole mobility of 1.5 $cm^2 V^{-1} s^{-1}$. Lee *et al.* synthesized a DPP-based polymer (PTDPPSe–Si) containing hybrid siloxane-solubilizing side chains.[141] The polymer films were annealed at different temperatures of 180, 220, and 260 °C. The as-spun film showed relatively broad (100) and (200) diffraction peaks. After annealing at 180, 220 or 260 °C, the (100) and (200) peaks became sharper along with the presence of a (300) peak. The film displayed the strongest (*h*00) peaks after annealing at 220 °C, which was determined as the optimal annealing temperature (Fig. 9a). As a result, OFETs based on the film annealed at 220 °C achieved the highest hole and electron mobilities of 1.69 and 0.2 $cm^2 V^{-1} s^{-1}$, respectively. In contrast, the as-spun film showed inferior hole and electron mobilities of 0.59 and 4.58×10^{-2} $cm^2 V^{-1} s^{-1}$, respectively. He *et al.* developed a novel bay-annulated indigo (BAI) based polymer (P1) from a natural dye (indigo) (Fig. 9b).[142] The polymer films were annealed at different temperatures of 50, 100, 150, 200, and 250 °C. 2D grazing incidence wide-angle X-ray scattering (2D-GIWAXS) tests at different temperatures were conducted under *in situ* annealing to study the crystallinity evolution (Fig. 9c and d). During the heating process, the diffraction peaks became stronger with

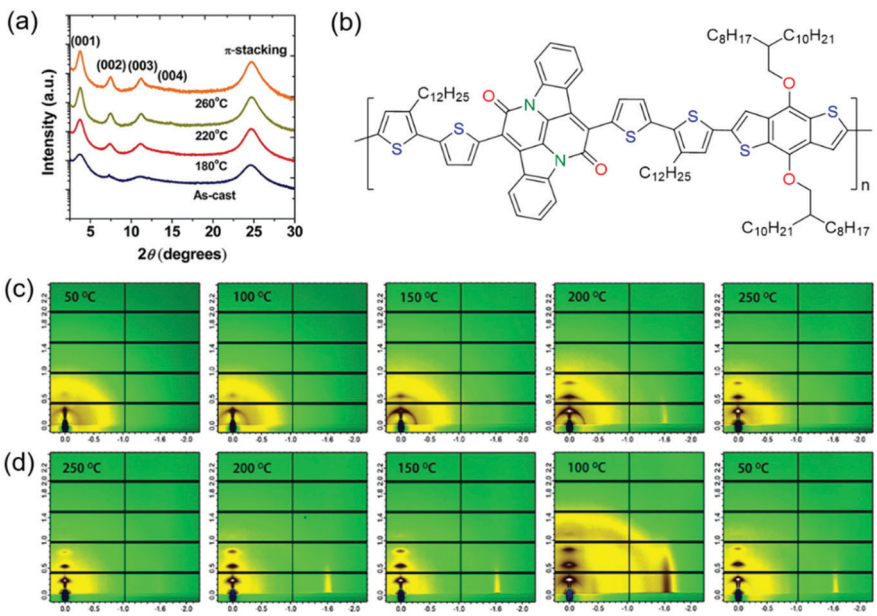

Fig. 9 Improving the crystallinity of CPs by thermal annealing. (a) XRD patterns of PTDPPSe–Si films depending on the annealing temperature. Reproduced with permission.[141] Copyright 2012, American Chemical Society. (b) The molecular structure of a BAI-based polymer (P1). GIWAXS patterns of P1 films during *in situ* (c) heating and (d) cooling cycles. Reproduced with permission.[142] Copyright 2014, American Chemical Society.

increasing annealing temperature. The films annealed below 150 °C showed weak (100) and (200) diffraction peaks. After annealing at 200 or 250 °C, the (100) and (200) peaks became stronger along with the presence of (300) and (010) peaks. During the cooling process, the diffraction peaks were retained. OFETs based on the annealed films achieved excellent ambipolar transport with hole and electron mobilities of 1.5 and 0.41 $cm^2 V^{-1} s^{-1}$, respectively.

In general, the as-spun polymer films are amorphous or display inferior crystallinity. Then thermal annealing is adopted to improve the crystallinity of polymer films. In an annealing process, the polymer chains can rearrange into long-range ordered packing modes controlled by the intermolecular interactions. There is an optimal annealing temperature for each polymer, which is confirmed by experiments. In general, the optimal annealing temperature is in the range from 100 to 250 °C. Note that the annealing temperature should be below the decomposition temperature of polymers.

4.2. Molecular mass modulation

Molecular mass of CPs is one of the important factors that can influence the crystallinity. For D–A CPs, increasing the number-average molecular mass (M_n) can improve the crystallinity. One possible explanation might be that the polymers with higher M_n have stronger D–A interactions, which could promote long-range ordered packing of the polymer molecules.[143]

Zhang *et al.* presented a D–A copolymer (CDT–BTZ) containing cyclopentadithiophene (CDT) as the donor and benzothiadiazole (BTZ) as the acceptor.[144] The polymer showed a low M_n of 10.2 kDa. WAXS characterization suggested that CDT–BTZ showed poor crystallinity with only one (010) diffraction peak. OFETs based on CDT–BTZ displayed a hole mobility of 0.11 $cm^2 V^{-1} s^{-1}$. In another study, Tsao *et al.* synthesized CDT–BTZ with a higher M_n of 50 kDa by improving the purity of the monomers.[145] This polymer displayed enhanced crystallinity with (100) and (010) diffraction peaks. As a result, the OFETs achieved better charge transport with a mobility of 0.67 $cm^2 V^{-1} s^{-1}$. Later, Tsao *et al.* synthesized several CDT–BTZs with various M_ns of 11, 18, 25, and 35 kDa (Fig. 10a).[143] XRD characterization suggested that the polymer crystallinity increased with the growing molecular weight. The polymer with the highest M_n showed the most intense (*h*00) diffraction peaks. One possible explanation might be that the polymer with a higher M_n had a stronger D–A interaction, which could promote higher order long-range packing of the polymer molecules. OFETs based on these polymers showed increasing hole mobilities from 0.28 $cm^2 V^{-1} s^{-1}$ for the lowest molecular weight sample (11 kDa) to 3.3 $cm^2 V^{-1} s^{-1}$ for the highest molecular weight sample (35 kDa). Li *et al.* synthesized DPP-based polymers (PDPP-TT) with various molecular masses by optimizing the polymerization reaction conditions.[146] The molecular masses of these polymers were 91, 344, and 501 kDa. XRD characterization indicated that all these polymers displayed (*h*00) diffraction peaks up to third order. However, the diffraction peak intensity significantly increased with increasing molecular weight. As a result, OFETs based on these polymers showed increasing hole mobilities from about 1 $cm^2 V^{-1} s^{-1}$ for the low molecular weight sample (91 kDa) to 9 $cm^2 V^{-1} s^{-1}$ for the high molecular weight

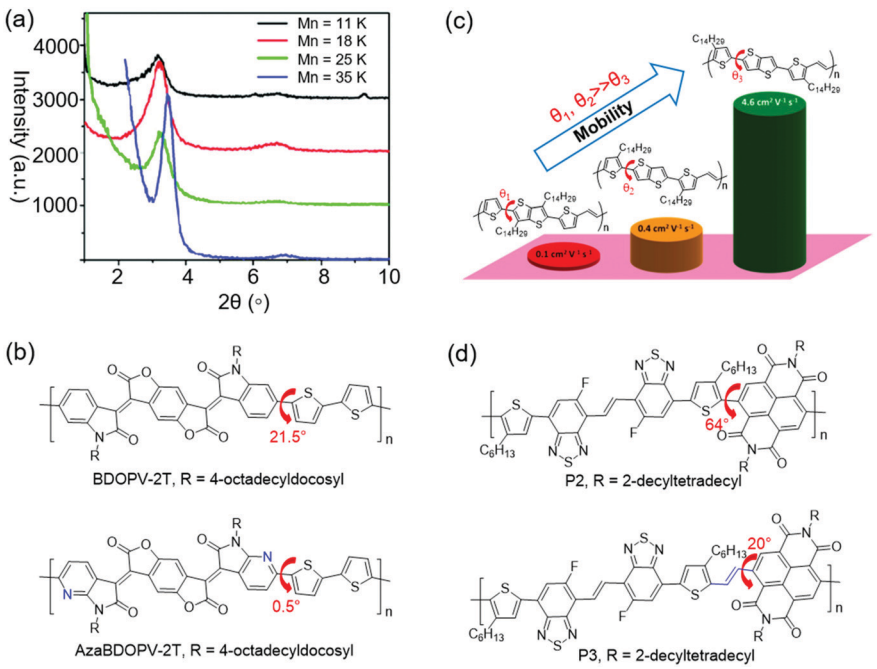

Fig. 10 Improving the crystallinity of CPs by molecular mass modulation or improving the planarity. (a) XRD patterns of CDT–BTZ depending on molecular mass. Reproduced with permission.[143] Copyright 2011, American Chemical Society. (b) The planarity variations by N substitution. (c) The planarity variations by adjusting the positions of side chains. Reproduced with permission.[151] Copyright 2014, American Chemical Society. (d) The planarity variations by adding a vinylene unit.

sample (501 kDa). These results clearly demonstrated that the as-synthesized polymers with high molecular masses were favorable for the achievement of high crystallinity and good semiconducting performance.

The crystallinity of CPs can be improved by optimizing the molecular mass. The optimal molecular mass can be confirmed by tuning the catalyst amount or polymerization time. Although larger molecular mass may improve crystallinity, it also decreases the solubility of CPs in chlorinated solvents, which will increase the difficulty of polymer processing. Therefore, the molecular mass should be controlled within an appropriate range.

4.3. Improving the planarity

Good backbone planarity of CPs is beneficial for intermolecular π–π stacking of polymer chains, thus improving the crystallinity.[143] The effective strategies include the introduction of sp^2-nitrogen atoms and vinylene units into polymers and so on.[147,148] For example, the replacement of C–H in aromatic rings with nitrogen atoms can decrease the steric hindrance, thus improving the coplanarity. Moreover, N atoms may induce intramolecular or intermolecular N···H and N···S interactions, which further improve the coplanarity. Fig. 10b–d show the crystallinity enhancement by improving the planarity.

Guo *et al.* reported the synthesis of 4,4′-dialkoxy-5,5′-bithiazole (BTzOR) and 3,3′-dialkoxy-2,2′-bithiophene (BTOR).[149] Incorporation of these building blocks into polymers afforded P1b and P4b, respectively. The replacement of (thiophene) C–H with (thiazole)N reduced the steric hindrance in –BTOR–Ar– units by eliminating C–H···H–C repulsions with adjacent arene units, thus enhancing the backbone coplanarity. The dihedral angle was about 23° between the alkoxythiophene and phthalimide planes in P4b, while it was 0° between the alkoxythiazole and phthalimide planes in P1b. The greater planarity in P1b was due to the elimination of C–H···H–C repulsions and the presence of S···O interactions in BTzOR units. XRD characterization indicated that the film of P4b was almost amorphous without diffraction peaks. However, the film of P1b showed a much more enhanced crystallinity with (*h*00) diffraction peaks up to third order. OFET devices based on P4b and P1b displayed hole mobilities of 0.04 and 0.13 $cm^2 V^{-1} s^{-1}$, respectively. The higher mobility of P1b could be attributed to the enhanced crystallinity endowed by the higher degree of backbone planarity. Dai *et al.* synthesized two polymers (BDOPV-2T and AzaBDOPV-2T) based on benzodifurandione-based oligo(*p*-phenylene vinylene) (BDOPV) and nitrogen-substituted BDOPV.[147,150] Incorporation of nitrogen atoms decreased the dihedral angle between the BDOPV and neighboring thiophene from 21.5° (BDOPV-2T) to 0.5° (AzaBDOPV-2T) (Fig. 10b). The enhanced planarity of AzaBDOPV-2T was attributed to the intramolecular N···S interactions and less steric hindrance of sp^2-N atoms than the CH units. 2D grazing-incidence X-ray diffraction (2D-GIXRD) characterization indicated that AzaBDOPV-2T achieved stronger diffraction peaks compared with BDOPV-2T. The π–π stacking distance of AzaBDOPV-2T (3.44 Å) was shorter than that of BDOPV-2T (3.55 Å). As a result, OFETs based on AzaBDOPV-2T demonstrated a remarkable electron mobility of 3.22 $cm^2 V^{-1} s^{-1}$, which was approximately two times that of the devices based on BDOPV-2T. Fei *et al.* designed three isomeric CPs (P1, P2 and P3), where the positions of alkyl chains on the polymer backbone were altered.[151] Density functional theory (DFT) calculations indicated that both P1 and P2 showed obvious torsional angles of 30.5° and 31.3° between the thiophene and thieno[3,2-*b*]thiophene moieties, while P3 adopted a good coplanar backbone with a dihedral angle of 3.7° between the two aromatics (Fig. 10c). The absorption maxima of P3 in solution and in film red-shifted compared to those of P1 and P2, suggesting that P3 had the best backbone planarity and the largest effective conjugation in these three polymers. The 2D-GIWAXS of P1 and P2 only displayed (100) diffraction peaks. In contrast, P3 showed (*h*00) diffraction peaks up to fourth order and a strong π–π stacking peak. The carrier mobilities of P1, P2, and P3 were 0.1, 0.4, and 4.6 $cm^2 V^{-1} s^{-1}$, respectively. The significant improvement in the transistor performance of P3 was consistent with its enhanced crystallinity. Wang *et al.* reported the synthesis of two polymers (P2 and P3) based on benzothiadiazole.[148] Intramolecular O···H hydrogen bonds formed in P3. DFT calculations indicated that P2 adopted a highly twisted backbone with a dihedral angle of 64° between the alkylated thiophene and neighboring NDI. P3 had additional vinylene bridges between NDI and thiophene units, resulting in a better backbone planarity due to the lower steric hindrance. The dihedral angle between the vinylene and NDI in P3 was 20° (Fig. 10d). The enhanced backbone planarity was beneficial for molecular packing. 2D-GIWAXS characterization indicated that both P2 and P3 showed second-order (*h*00) and (010) diffraction peaks. However, the (*h*00) diffraction peak intensity of P3 was stronger than that of P2. Moreover, the π–π stacking distance of P3 was much shorter than that of P2. OFETs based on P3 displayed an electron mobility of 3.95 $cm^2 V^{-1} s^{-1}$, which was one order of magnitude higher than P2.

Generally, functional groups (CN, CH_3, Br, *etc.*) with large steric hindrance in CPs can hinder the molecular packing, which is harmful for polymer crystallization. Therefore, the crystallinity of CPs can be improved by introducing functional groups with small steric hindrance into the polymer backbone. These groups include sp^2-N atoms and vinylene units. The introduction of sp^2-N atoms not only decrease the steric hindrance, but also induce intermolecular N···H and N···S interactions, both of which can improve the crystallinity. Despite the aforementioned advantages, it is difficult to synthesize *N*-substituted units, especially for *N*-substituted acceptors.[147] More effective synthetic approaches for *N*-substituted polymers should be explored in the future.

4.4. Molecular geometry modulation

Molecular geometric structures of the polymer backbone can have a remarkable effect on the crystallinity. Molecular geometric structures include molecular symmetry, regularity, and linearity. Recent studies indicate that polymers with centrosymmetric or regioregular monomers generally showed improved crystallinity than their counterparts with axisymmetric or regiorandom ones.[152–154] A linear polymer backbone instead

of a curved one is beneficial for polymer crystallization.[155] The reason might be that regioregular and linear polymers can form better intermolecular π–π stacking in the solid state, thus improving the crystallinity. Fig. 11 shows the examples of molecular geometry modulation to improve the crystallinity.

The effect of molecular symmetry and regularity on crystallinity has been investigated. Lei *et al.* developed two D–A CPs (IIDDT and IIDT), which contained centrosymmetric acceptors (isoindigo).[156] However, the centrosymmetric donor (bithiophene) was found for IIDDT, while the axisymmetric one (thiophene) was found for IIDT. Since the symmetry of donors had a remarkable effect on the polymer crystallinity, the film based on IIDT displayed a relatively amorphous structure with one weak diffraction peak, while the film based on IIDDT showed a much more enhanced crystallinity with (*h*00) diffraction peaks up to fourth order. Consequently, IIDDT-based FETs provided a hole mobility of 0.79 $cm^2 V^{-1} s^{-1}$, which was one order of magnitude higher than IIDT-based devices. Later, Lei *et al.* synthesized ten isoindigo-based polymers containing centrosymmetric or axisymmetric donors to systematically study the influence of symmetry and backbone curvature on crystallinity and semiconductor properties (Fig. 11a).[152] Different from the polymers containing axisymmetric donors, the polymers containing centrosymmetric ones showed a linear backbone for good interchain π–π stacking interactions. The 2D-GIXRD of polymers containing centrosymmetric donors displayed fourth-order (*h*00) diffraction peaks. However, all polymers containing axisymmetric donors showed poor crystallinity with one or no (*h*00) diffraction peak. As a result, OFETs based on these six polymers containing centrosymmetric donors demonstrated hole-transporting behaviors with mobilities exceeding 0.1 $cm^2 V^{-1} s^{-1}$, which were one or three orders of magnitude higher than those of the devices based on the polymers with axisymmetric donors. These results demonstrated that designing polymers containing both centrosymmetric acceptors and donors was favorable for the achievement of high crystallinity and good semiconducting performance. Ying *et al.* developed two regioregular copolymers (P1 and P2) and one regiorandom copolymer (P3) based on pyridal[2,1,3]thiadiazole (PT) units (Fig. 11b).[153] The optical band gaps of P1 and P2 were smaller than that of P3, indicating that molecular regioregularity could decrease the band gap of the polymers. Moreover, the backbone regioregularity had a direct impact on the molecular packing of the polymer films. 2D-GIWAXS characterization indicated that P1 and P2 showed stronger (*h*00) diffraction peaks compared with P3. Consequently, the regioregular polymers (P1 and P2) demonstrated remarkable hole mobilities of 0.4 and 0.6 $cm^2 V^{-1} s^{-1}$, respectively, which were two orders of magnitude higher than that of the regiorandom polymer (P3). Wang *et al.* reported the synthesis of a regioregular polymer (P2F) and a regiorandom polymer (PRF) based on 5-fluorobenzo[*c*][1,2,5]thiadiazole units.[157] As shown in 2D-GIWAXS, films of both P2F and PRF displayed third-order (*h*00) diffraction peaks and π–π stacking peaks. However, the diffraction peak intensity of P2F was stronger than that of PRF. The regiorandom polymer PRF showed a hole mobility of 0.4 $cm^2 V^{-1} s^{-1}$, while its regioregular counterpart P2F achieved a mobility of 1.2 $cm^2 V^{-1} s^{-1}$. The significant improvement in the transistor performance of P2F was attributed to the enhanced crystallinity.

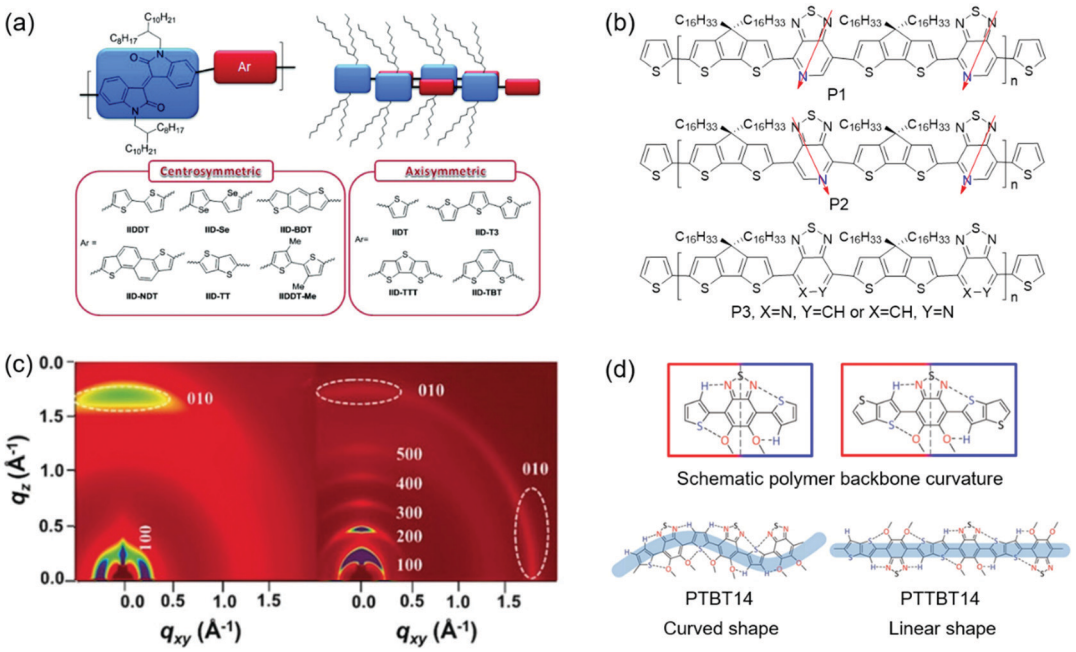

Fig. 11 Improving the crystallinity of CPs by molecular geometry modulation. (a) The molecular structures of isoindigo-based polymers containing centrosymmetric and axisymmetric units. Reproduced with permission.[152] Copyright 2012, American Chemical Society. (b) The molecular structures of regioregular polymers (P1 and P2) and a regiorandom polymer (P3). (c) 2D-GIWAXS of s-BTI2-FT (left) and f-BTI2-FT (right). Reproduced with permission.[158] Copyright 2017, Wiley-VCH. (d) The molecular structures of two polymers (PTBT14 and PTTBT14) with different backbone curvatures. Reproduced with permission.[159] Copyright 2014, American Chemical Society.

Molecular linearity of the polymer backbone can have a remarkable effect on the crystallinity. Rieger *et al.* designed five polymers (P1–P5) containing different benzodithiophene isomers with varying degrees of curvature.[155] The backbones of P1–P3 were linear, while those of P4 and P5 were curved. The influence of the curvature on optical gaps and crystallinity was systematically investigated. UV-vis spectroscopy indicated that the optical gaps of the polymers became larger with increasing curvature due to decreased effective conjugation lengths. Wide-angle XRD experiments suggested that the linear polymers displayed enhanced crystallinity compared with the curved ones. For example, P3 showed strong third-order (*h*00) and (010) diffraction peaks, while P4 and P5 only displayed weak (100) and (010) diffraction peaks. As a result, the carrier mobilities of P1, P2, and P3 were one order of magnitude higher than those of P4 and P5. These results demonstrated that designing polymers with a linear backbone was favorable for the achievement of high crystallinity and good semiconducting performance. Wang *et al.* designed two bithiophene imide (BTI)-based n-type copolymers (s-BTI2-FT and f-BTI2-FT).[158] s-BTI2-FT possessed a BTI dimer connected through a single bond, while f-BTI2-FT contained a fused BTI dimer. DFT calculations revealed that the molecular shapes of s-BTI2-FT and f-BTI2-FT were sinewave and pseudo-linear, respectively. f-BTI2-FT possessed a more linear backbone than s-BTI2-FT. The 2D-GIXRD of s-BTI2-FT showed (100) and (010) diffraction peaks. However, f-BTI2-FT displayed enhanced crystallinity with pronounced fifth-order (*h*00) diffraction peaks and a (010) peak (Fig. 11c). OFETs based on f-BTI2-FT showed an electron mobility of 1.13 $cm^2 V^{-1} s^{-1}$, which was higher than that of OFETs based on s-BTI2-FT. Lee *et al.* reported thiophene and thienothiophene based copolymers (PTBT14 and PTTBT14) with different backbone curvatures.[159] DFT calculations indicated that both polymers possessed a similar planar structure *via* intramolecular noncovalent C–H···N and S···O attractive interactions. However, PTTBT14 was a linear polymer, while PTBT14 was a curved one (Fig. 11d). The linearity of the polymer backbone significantly influenced the crystallinity of polymer films. The film of PTBT14 annealed at 200 °C only showed weak (100) and (200) diffraction peaks. In contrast, the annealed film of PTTBT14 displayed pronounced third-order (*h*00) diffraction peaks and a π–π stacking peak. The carrier mobilities of PTBT14 and PTTBT14 were 0.3 and 1.2 $cm^2 V^{-1} s^{-1}$, respectively. The improvement in the mobility of PTTBT14 was consistent with its enhanced crystallinity.

Molecular geometric structures of CPs can influence the molecular packing in film, thus affecting the crystallinity. It has been demonstrated that the crystallinity can be improved by designing polymers with centrosymmetric, regioregular, and linear monomers.[152–155] Different from other factors that can influence the crystallinity, molecular geometry, especially for molecular linearity, is generally ignored. Therefore, molecular geometry of CPs should be paid more attention when designing new polymers with high crystallinity.

4.5. Side chain engineering

CPs generally contain side chains, which not only endow the polymers with solubility in organic solvents, but also affect the intermolecular packing and thus the crystallinity. The side chain engineering strategy includes the optimization of the branched point position of side chains and the introduction of semifluorinated or hydrogen bond-containing alkyl chains and so on.[160–164] This strategy can improve the polymer crystallinity by enhancing the intermolecular interactions. For instance, the strong self-organization behaviors of the semifluorinated alkyl chains can promote the polymer molecules to form a long-range crystalline structure.[163] Yang *et al.* provided a good review of the side-chain modulation strategy for OFETs.[165] Fig. 12a

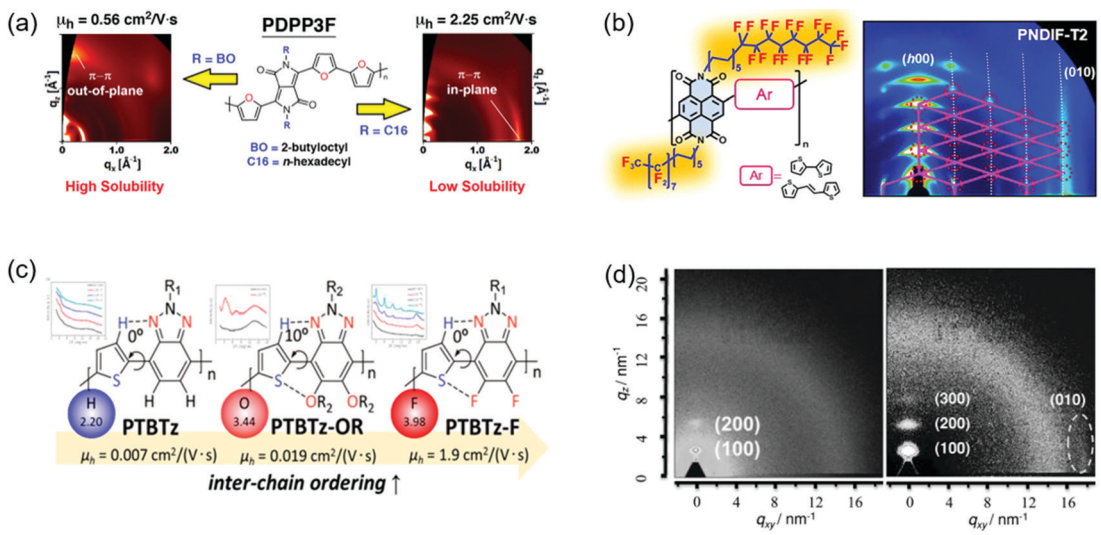

Fig. 12 Improving the crystallinity of CPs by side chain engineering and fluorine substitution. (a) GIXRD patterns of PDPP3F containing different side chains. Reproduced with permission.[167] Copyright 2013, American Chemical Society. (b) The molecular structures and GIXRD patterns of NDI-based polymers containing semifluorinated side chains. Reproduced with permission.[163] Copyright 2016, American Chemical Society. (c) The molecular structures of benzotriazole-based polymers containing different substituted atoms. Reproduced with permission.[171] Copyright 2014, American Chemical Society. (d) 2D GIWAXS of the annealed films of PDPP-TVT (left) and PDPP-4FTVT (right). Reproduced with permission.[172] Copyright 2015, Wiley-VCH.

and b show some examples of side chain engineering to improve the crystallinity.

Kang *et al.* developed four DPP-based polymers (P-24DPPDBTE, P-24-DPPDTSE, P-29DPPDBTE, and P-29-DPPDTSE).[166] Compared with P-24DPPDBTE and P-24-DPPDTSE (P-24s), P-29DPPDBTE and P-29-DPPDTSE (P-29s) possessed extended branching-position-adjusted alkyl chains, which were favorable for molecular packing. XRD characterization suggested that the crystallinity of P-29s was much more improved than P-24s. For example, P-24DPPDBTE showed weak (100) and (200) diffraction peaks, whereas P-29DPPDBTE displayed pronounced (*h*00) diffraction peaks up to fourth order. The π–π stacking distance of P-29DPPDBTE was much shorter than that of P-24DPPDBTE. As a result, P-29s showed better charge transport compared with P-24s. Particularly, P-29-DPPDTSE achieved a remarkable hole mobility of 12.04 $cm^2 V^{-1} s^{-1}$, which was about three times that of P-24-DPPDTSE. Chen *et al.* reported two furan-containing DPP-based polymers (PDPP3F-BO and PDPP3F-C16).[167] PDPP3F-BO and PDPP3F-C16 contained branched 2-butyloctyl and linear *n*-hexadecyl side chains, respectively (Fig. 12a). The linear side chains were expected to enhance the polymer crystallinity due to the less steric hindrance for molecular packing. 2D-GIXRD characterization indicated that PDPP3F-BO showed poor crystallinity with (100) and (200) diffraction peaks. In contrast, PDPP3F-C16 displayed strong fourth-order (*h*00) diffraction peaks. Compared with PDPP3F-BO, PDPP3F-C16 achieved tighter π–π stacking with a shorter distance. OFETs based on PDPP3F-C16 demonstrated a high hole mobility of 2.25 $cm^2 V^{-1} s^{-1}$, which was about four times that of the device based on PDPP3F-BO. Wang *et al.* developed two DPP-based polymers (PDPPSe-10 and PDPPSe-12) containing both branched and linear alkyl chains.[168] A polymer (PDPPSe) only containing branched alkyl chains was synthesized for comparison. The replacement of bulky branched alkyl chains with linear ones could reduce the steric hindrance, thus improving the backbone planarity. 2D-GIWAXS characterization indicated that PDPPSe showed poor crystallinity with (100) and (200) diffraction peaks. In contrast, PDPPSe-10 and PDPPSe-12 displayed clear fourth-order (*h*00) diffraction peaks. OFETs based on PDPPSe-10 and PDPPSe-12 achieved hole mobilities of 8.1 and 9.4 $cm^2 V^{-1} s^{-1}$, respectively, which were about six times that of the devices based on PDPPSe.

The introduction of semifluorinated or hydrogen bond-containing alkyl chains can also improve the crystallinity of CPs. Kang *et al.* developed two novel NDI-based polymers (PNDIF-T2 and PNDIF-TVT) containing linear semifluorinated side chains (Fig. 12b).[163] Two polymers (PNDI2OD-T2 and PNDI2DT-TVT) containing branched alkyl chains were synthesized for comparison. The strong self-organization behaviors of the semifluorinated chains induced a high degree of long-range order in the polymer backbone by forming a superstructure composed of "backbone crystals" and "side-chain crystals". The annealed films of PNDIF-T2 and PNDIF-TVT displayed much more enhanced crystallinity compared with those of PNDI2OD-T2 and PNDI2DT-TVT. For example, PNDI2OD-T2 only showed (100), (200), and (010) diffraction peaks, while PNDIF-T2 displayed clear (*h*00) peaks up to fifth order and an intense (010) peak. Moreover, (00*l*), (30*l*), and (501) peaks were found for PNDIF-T2. All these peaks suggested the superior crystallinity of PNDIF-T2. As a result, OFETs based on PNDIF-T2 and PNDIF-TVT achieved outstanding electron mobilities of 3.95 and 3.75 $cm^2 V^{-1} s^{-1}$, respectively, which were much higher than those of PNDI2OD-T2 and PNDI2DT-TVT. Heo *et al.* reported two thienylenevinylene (TV) based polymers (PC12TVC5F7T and PC12TV12T) containing semi-fluorinated alkyl and hydrocarbon alkyl side chains.[169] Highly crystalline structures formed in PC12TVC5F7T films through strong intermolecular interactions between semi-fluorinated alkyl chains. 2D-GIWAXS characterization indicated that PC12TVC5F7T exhibited intense (*h*00) diffraction peaks up to fifth order and a (010) peak. Several (00*l*) peaks were also observed for PC12TVC5F7T. Moreover, AFM images revealed that PC12TVC5F7T films displayed well-defined plate-like morphology with a domain size of about 40 nm. In contrast, PC12TV12T only showed (*h*00) peaks up to third order. OFET devices based on PC12TVC5F7T and PC12TV12T displayed hole mobilities of 1.91 and 1.05 $cm^2 V^{-1} s^{-1}$, respectively. The higher mobility of PC12TVC5F7T could be attributed to the improved crystallinity endowed by semi-fluorinated alkyl chains. Yao *et al.* designed three DPP-based polymers (pDPP4T-1, pDPP4T-2, and pDPP4T-3), in which the proportions of the branched alkyl chains and urea-containing alkyl chains were 30 : 1, 20 : 1, and 10 : 1, respectively.[164] Fourier transform infrared and ^1H NMR spectra demonstrated that the urea-containing alkyl chains could induce intermolecular hydrogen bonds. The number of hydrogen bonds increased from pDPP4T-1 to pDPP4T-3. GIXRD indicated that the diffraction peak intensity of the out-of-plane (*h*00) and in-plane (010) peaks increased from pDPP4T-1 to pDPP4T-3. As a result, pDPP4T-3 achieved the highest hole mobility of 13.1 $cm^2 V^{-1} s^{-1}$ among the polymers.

The side chains of CPs can have a remarkable effect on the crystallinity. The crystallinity of CPs can be improved by optimizing the branched point position of side chains or introducing semifluorinated chains and hydrogen bond-containing chains. The introduction of semifluorinated chains or hydrogen bond-containing chains can enhance the intermolecular interactions of CPs by strong self-organization or hydrogen bond interactions, which will promote the polymer crystallization.[163,164] However, the optimal branched point positions of side chains vary for different polymers, which needs to be confirmed by experiments. Therefore, the side chains of CPs should be carefully selected to achieve good crystallinity.

4.6. Fluorine substitution

Fluorine substitution in the polymer backbone is an effective approach to improve the crystallinity. Fluorine atom is a strong electron-withdrawing unit with a small van der Waals radius (1.35 Å). The introduction of fluorine atoms can induce intramolecular or intermolecular F···S and F···H noncovalent interactions, which may improve the backbone planarity. Both noncovalent interactions and better planarity can improve the polymer crystallinity. Fig. 12c and d show some examples of fluorine substitution strategies to improve the crystallinity.

Lei *et al.* presented a fluorinated (FBDPPV-1) and a non-fluorinated polymer (BDPPV) based on BDOPV units.[170]

Theoretical calculations indicated that FBDPPV-1 showed an almost planar conjugated backbone. Both polymer films exhibited strong out-of-plane (*h*00) diffraction peaks with edge-on lamellar packings. FBDPPV-1 displayed pronounced fifth-order (*h*00) diffraction peaks, whereas BDPPV displayed only fourth-order (*h*00) peaks. FBDPPV-1 showed a stronger (010) diffraction peak with a shorter π–π stacking distance of 3.42 Å compared with BDPPV. In addition, the root-mean-square (RMS) analysis of the AFM height figures indicated that the film of FBDPPV-1 showed a larger surface roughness compared with BDPPV. Both 2D-GIXRD and AFM data demonstrated that fluorination in polymers could improve the crystallinity. The electron mobilities of BDPPV and FBDPPV-1 were 1.1 and 1.7 $cm^2 V^{-1} s^{-1}$, respectively. The improvement in the mobility of FBDPPV-1 was consistent with its enhanced crystallinity. In another study, Yum *et al.* developed three functionalized benzotriazole-based polymers (PTBTz, PTBTz-OR, and PTBTz-F) (Fig. 12c).[171] The dihedral angles between the thiophene and the benzotriazole units in PTBTz, PTBTz-OR, and PTBTz-F were 0°, 10°, and 0°, respectively. In PTBTz, only N···H noncovalent interactions were observed. In contrast, N···H and S···O or S···F noncovalent interactions were observed for PTBTz-OR or PTBTz-F. These noncovalent interactions were likely to induce strong intermolecular packing. XRD characterization indicated that PTBTz showed only a weak (100) diffraction peak, while PTBTz-OR or PTBTz-F displayed second- or fourth-order (*h*00) diffraction peaks. Moreover, both PTBTz-OR and PTBTz-F showed π–π stacking peaks. The hole mobilities of PTBTz, PTBTz-OR, and PTBTz-F were 0.007, 0.019, and 1.9 $cm^2 V^{-1} s^{-1}$, respectively. The highest mobility of PTBTz-F was consistent with its best crystallinity. Gao *et al.* developed a polymer (PDPP-4FTVT) based on tetrafluorinated (*E*)-2-(2-(thiophen-2-yl)vinyl)thiophene (TVT) *via* direct arylation polycondensation.[172] A non-fluorinated polymer (PDPP-TVT) was also synthesized for comparison. DFT calculations revealed that PDPP-4FTVT showed a completely planar backbone due to the presence of intramolecular F···S noncovalent interactions. The film of PDPP-4FTVT annealed at 200 °C displayed obvious third-order (*h*00) diffraction peaks and a (010) peak. In contrast, the annealed film of PDPP-TVT exhibited only relatively weak (100) and (200) diffraction peaks without a (010) peak (Fig. 12d). OFETs based on PDPP-4FTVT showed an ambipolar transport with hole and electron mobilities of 3.40 and 5.86 $cm^2 V^{-1} s^{-1}$, respectively, which were higher than those of PDPP-TVT. Wang *et al.* designed three polymers (PhF0, PhF1, and PhF2,5) containing fluorinated phenyl units with increasing number of F atoms (0, 1, 2F).[173] Theoretical calculations indicated that the backbone planarity of PhF2,5 was enhanced compared with PhF0 and PhF1. 2D-GIWAXS characterization indicated that the films of PhF0 and PhF1 were almost amorphous. In contrast, the film of PhF2,5 displayed (*h*00) diffraction peaks up to third order. A strong π–π stacking peak was also observed in the in-plane direction. The carrier mobility values of the polymers increased with substitution of more fluorine atoms. PhF2,5 displayed a hole mobility of 0.92 $cm^2 V^{-1} s^{-1}$, which was three orders of magnitude higher than that of PhF0. Sun *et al.* reported a general synthetic approach to obtain methoxylated quinoidal bithiophene (MQBT) units with a single regioisomer.[174] A fluorinated (P2FMQBT-DFBT) and a non-fluorinated (PMQBT-BT) polymer based on MQBT units were prepared. DFT calculations suggested that P2FMQBT-DFBT possessed a better planar backbone compared with PMQBT-BT. 2D-GIXRD characterization indicated that PMQBT-BT showed a weak (100) diffraction peak, while P2FMQBT-DFBT displayed a much more enhanced crystallinity with (*h*00) diffraction peaks up to third order. Moreover, P2FMQBT-DFBT had a stronger (010) diffraction peak with a much shorter π–π stacking distance of 3.59 Å compared with PMQBT-BT. As a result, P2FMQBT-DFBT showed a hole mobility of 2.7 $cm^2 V^{-1} s^{-1}$, which was one order of magnitude higher than that of PMQBT-BT.

Fluorine substitution is a widely used method for improving the crystallinity of CPs. The introduction of fluorine atoms can enhance the intermolecular interactions of CPs by F···S and F···H noncovalent interactions, which will promote the polymer crystallization. Various fluorinated polymers or even multifluorinated polymers have been developed and achieved good crystallinity.[175] However, it is very challenging to synthesize fluorinated polymers.[172] Facile and effective synthetic methods for fluorinated polymers are highly desired. Except for fluorination, other halogenation methods like chlorination can be adopted to improve the crystallinity, which remains to be explored.

4.7. Single crystals of conjugated polymers

CPs generally contain branched alkyl chains, which are unfavorable for polymer crystallization. Also, the Suzuki or Stille polymerization reactions are irreversible. As a result, the as-synthesized polymers normally are polycrystalline rather than single-crystalline. Since single crystals of CPs offer a perfect platform to study the structure–property relationship and investigate the charge transport mechanisms in polymer systems, it is highly desirable to grow such single crystals. Moreover, polymer crystals usually exhibit better semiconducting performance than films due to the long-range ordered molecular packing. However, conjugated polymer crystals amenable to single-crystal XRD are still in the early stage. Most of the reported polymer crystals are obtained by a self-assembly method as nanowires or microwires.[65,66] Fig. 13 shows the reported polymer crystals.

Rahimi *et al.* obtained large single crystals of a regioregular poly(3-hexylthiophene) polymer (P3HT-26) by a self-seeding method (Fig. 13a).[176] This method contained three steps: dissolution, seed forming at a seeding temperature (T_{SS}), and crystal growth at a lower temperature (T_C). Large single crystals with a length of 20 μm were obtained by precisely controlling T_{SS} and T_C. SAED indicated that single crystals had a monoclinic crystal structure. The π–π stacking distance was 4.3 Å. Single crystals of P3HT samples with other molecular weights (P3HT-4 and P3HT-5) were also obtained by this method. Kim *et al.* reported single crystal nanowires based on a copolymer (PDTTDPP) of DPP and dithieno[3,2-*b*:2′,3′-*d*]thiophene (DTT) by a self-assembly method.[177] The molecular rigidity and

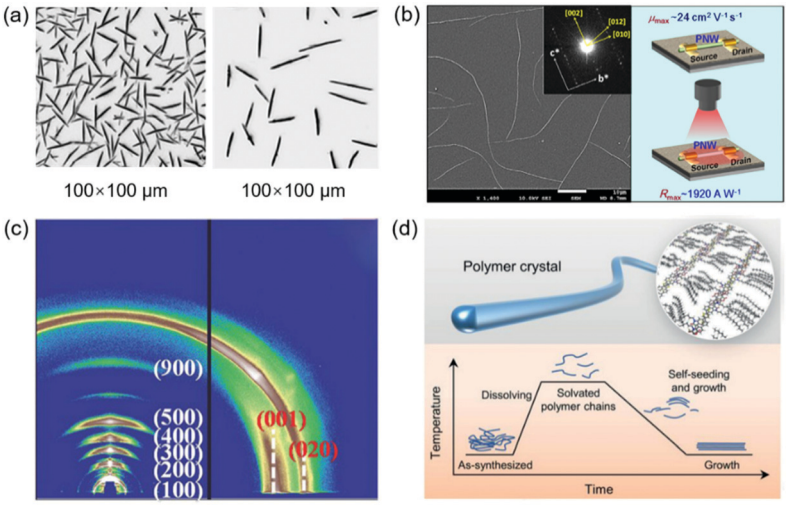

Fig. 13 Conjugated polymer crystals. (a) Optical micrographs of the single crystals of P3HT-26. Reproduced with permission.[176] Copyright 2012, Wiley-VCH. (b) Polymer nanowires of DPPBTSPE and its applications in electronic devices. Reproduced with permission.[65] Copyright 2015, American Chemical Society. (c) GIXRD patterns of poly-PCDA crystals. Reproduced with permission.[178] Copyright 2017, Wiley-VCH. (d) 3D schematic of the polymer crystals by a self-seeding approach. Reproduced with permission.[66] Copyright 2021, Wiley-VCH.

planarity of DTT could enhance intermolecular interactions to promote the self-assembly of the polymer backbone. The polymer nanowires (PNWs) were obtained by storing the dissolved polymer solution at room temperature for several days. The PNWs displayed a small curvature and surface uniformity with an average length of 15.9 μm and a width of 65 nm. SAED patterns indicated that the PNWs showed highly crystalline nature with an orthorhombic crystal structure. OFETs based on PNWs achieved a remarkable hole mobility of 7.0 $cm^2 V^{-1} s^{-1}$, which was one order of magnitude higher than that of the devices based on spin-coated films. Um *et al.* synthesized two fractions of DPPBTSPE with high and low number-average molecular weights (MW) of 8 and 68 kDa, respectively (Fig. 13b).[65] Both high- and low-MW polymers could form single-crystalline nanowires by a self-assembly method. However, only the low-MW polymer formed well-isolated nanowires with a higher aspect ratio, which could be applied to fabricate single nanowire-based devices. The isolated nanowires had lengths of 50–100 μm and widths of 170 nm. The nanowires showed highly crystalline nature with an orthorhombic crystal structure. 2D-GIXRD characterization indicated that the single-crystalline nanowires displayed enhanced crystallinity compared with spin-coated films. The (010) diffraction peak of nanowires was stronger and sharper than that of spin-coated films. As a result, OFETs based on nanowires achieved a superior hole mobility of 24 $cm^2 V^{-1} s^{-1}$, which was one order of magnitude higher than that of the devices based on spin-coated films. Yao *et al.* achieved polymer nanocrystals by an *in situ* topochemical polymerization method.[178] Firstly, single crystals of 10,12-pentacosadiynoic acid (PCDA) were obtained in a physical vapor transport (PVT) system. Then, single crystals of PCDA were directly transformed into poly-PCDA crystals by white light irradiation. The length and width of poly-PCDA crystals were tens of micrometers and hundreds of nanometers, respectively. The poly-PCDA crystals showed highly crystalline nature and long-range order with an orthorhombic crystal structure. 2D-GIXRD characterization indicated that poly-PCDA crystals displayed intense (*h*00), (020), and (001) diffraction peaks (Fig. 13c). SAED of poly-PCDA crystals showed very sharp diffraction spots, suggesting the high degree of crystallinity of this polymer. As a result, OFETs based on poly-PCDA crystals achieved outstanding charge transport with a maximum mobility of 50 $cm^2 V^{-1} s^{-1}$. Yao *et al.* reported a facile approach to obtain microwire crystals of a benzodifurandione-based oligo(*p*-phenylene vinylene) polymer (F_4BDOPV-2T) by a controlled self-seeding growth process.[66] The self-seeding approach contained three steps: dissolution at 140 °C, self-seeding and growth through slow cooling, and further crystal growth at room temperature (Fig. 13d). The obtained polymer crystals displayed a microwire shape with a length of 40 μm and a width of 0.5–7 μm. PXRD patterns of the polymer crystals showed intense diffraction peaks, which was consistent with Pawley-simulated XRD data. However, some diffraction peaks (0.5–1.5 Å) disappeared in the GIWAXS patterns of spin-coated polymer films. These results indicated the improved crystallinity in microwire crystals than in thin films. As a result, OFETs based on microwire crystals demonstrated a remarkable electron mobility of 3.46 $cm^2 V^{-1} s^{-1}$, which was about four times that of the devices based on spin-coated films. To demonstrate the generality of this method, another n-type polymer (P(NDI2OD-T2)) was selected for crystal growth. P(NDI2OD-T2) microwire crystals displayed an electron mobility of 2.56 $cm^2 V^{-1} s^{-1}$, which was much higher than that of P(NDI2OD-T2) films.

To date, conjugated polymer crystals have been achieved by a self-assembly method, which mainly contains three steps: polymer dissolution, seed forming, and crystal growth.[66,176] The obtained polymer crystals by this method are nanowires or microwires, which have been demonstrated to exhibit a much better semiconducting performance than films in OFET applications.[66] However, large-sized polymer crystals amenable

to single-crystal XRD have not been achieved, which need further studies. It may be a feasible way to synthesize polymer single crystals by adopting reversible polymerization reactions.

5. Conclusion and outlook

Crystallinity of COFs and CPs is of great importance for structural determination and practical applications. The enhancement of crystallinity can significantly improve the performance of COFs and CPs in photocatalysis, electronics, and other fields. In recent years, diverse design strategies have been developed to improve the crystallinity of COFs and CPs. The key point for improving the crystallinity and even achieving single crystals is to modulate the reversible process during the bond formation, offering enough time for self-correction of defects. For COFs, the strategies include polycondensation reaction optimization, improving the planarity, hydrogen bond and fluorine substitution, and so on. For CPs, the strategies include thermal annealing, molecular mass modulation, improving the planarity, molecular geometry modulation, side chain engineering, fluorine substitution, and so on. To date, CP crystals and COF single crystals have been achieved based on the above effective strategies. However, there are still several fundamental issues that need further studies.

It is well known that the polycondensation reaction conditions can have significant effects on the crystallinity of COFs. The relationship between the polycondensation reaction conditions and the crystallinity is complicated and requires further studies. Although single-crystal COFs have been achieved, more universal synthetic methods to obtain single crystals are still desired to offer precise structural information of COFs. Moreover, the reported single-crystal COFs are mainly based on boronate ester formation and Schiff base reactions. Single-crystal COFs based on other reactions remain to be explored.[4] Although the effect of single-crystal size on the gas absorption properties was recently investigated,[132] it is still very interesting to explore the applications of single-crystal COFs in other fields such as transistors and luminescent devices. For CPs, nitrogen or fluorine substitution can improve the crystallinity. However, it is difficult to synthesize the monomers containing nitrogen or fluorine atoms.[172,179] Despite the fact that various strategies have been developed to improve the crystallinity of CPs, the polymer crystals amenable to single-crystal XRD are still in the early stage. Clearly, it is very difficult to obtain single crystals of the reported polymers synthesized based on irreversible coupling reactions. Thus, adopting reversible reactions may promote the realization of polymer single crystals.

Despite the challenges remaining for the crystallinity of COFs and CPs, various strategies have been demonstrated to be effective to achieve highly crystalline COFs and CPs. These strategies can also be applied in other new polymers, especially for those that are difficult to crystallize. The highly crystalline COFs and CPs will be attractive for practical applications, which can provide feasible solutions to address energy and environment issues.

Conflicts of interest

There are no conflicts to declare.

Acknowledgements

QZ acknowledges the support of starting funds from City University of Hong Kong.

References

1 A. P. Côté, A. I. Benin, N. W. Ockwig, M. O'Keeffe, A. J. Matzger and O. M. Yaghi, *Science*, 2005, **310**, 1166–1170.
2 H. M. El-Kaderi, J. R. Hunt, J. L. Mendoza-Cortés, A. P. Côté, R. E. Taylor, M. O'Keeffe and O. M. Yaghi, *Science*, 2007, **316**, 268–272.
3 C. S. Diercks and O. M. Yaghi, *Science*, 2017, **355**, 6328.
4 E. Jin, M. Asada, Q. Xu, S. Dalapati, M. A. Addicoat, M. A. Brady, H. Xu, T. Nakamura, T. Heine, Q. Chen and D. Jiang, *Science*, 2017, **357**, 673–676.
5 C. K. Chiang, C. R. Fincher, Y. W. Park, A. J. Heeger, H. Shirakawa, E. J. Louis, S. C. Gau and A. G. MacDiarmid, *Phys. Rev. Lett.*, 1977, **39**, 1098–1101.
6 (*a*) A. Tsumura, H. Koezuka and T. Ando, *Appl. Phys. Lett.*, 1986, **49**, 1210–1212; (*b*) Y. Zhi, Z. Wang, H.-L. Zhang and Q. Zhang, *Small*, 2020, **16**, 2001070.
7 H. Yan, Z. Chen, Y. Zheng, C. Newman, J. R. Quinn, F. Dotz, M. Kastler and A. Facchetti, *Nature*, 2009, **457**, 679–686.
8 J. W. Colson and W. R. Dichtel, *Nat. Chem.*, 2013, **5**, 453–465.
9 R.-R. Liang, S.-Y. Jiang, A. Ru-Han and X. Zhao, *Chem. Soc. Rev.*, 2020, **49**, 3920–3951.
10 X. Guan, F. Chen, Q. Fang and S. Qiu, *Chem. Soc. Rev.*, 2020, **49**, 1357–1384.
11 J. D. Yuen and F. Wudl, *Energy Environ. Sci.*, 2013, **6**, 392–406.
12 Y. Jin, Y. Hu and W. Zhang, *Nat. Rev. Chem.*, 2017, **1**, 0056.
13 J.-S. M. Lee and A. I. Cooper, *Chem. Rev.*, 2020, **120**, 2171–2214.
14 D. Rodríguez-San-Miguel and F. Zamora, *Chem. Soc. Rev.*, 2019, **48**, 4375–4386.
15 X.-H. Liu, C.-Z. Guan, D. Wang and L.-J. Wan, *Adv. Mater.*, 2014, **26**, 6912–6920.
16 S. Kandambeth, K. Dey and R. Banerjee, *J. Am. Chem. Soc.*, 2019, **141**, 1807–1822.
17 S. Seth and S. Jhulki, *Mater. Horiz.*, 2021, **8**, 700–727.
18 X. Huang, C. Sun and X. Feng, *Sci. China: Chem.*, 2020, **63**, 1367–1390.
19 S. Z. Bisri, C. Piliego, J. Gao and M. A. Loi, *Adv. Mater.*, 2014, **26**, 1176–1199.
20 J. Yang, Z. Zhao, S. Wang, Y. Guo and Y. Liu, *Chem*, 2018, **4**, 2748–2785.
21 H. Huang, L. Yang, A. Facchetti and T. J. Marks, *Chem. Rev.*, 2017, **117**, 10291–10318.

22 A. J. Heeger, *Chem. Soc. Rev.*, 2010, **39**, 2354–2371.
23 Z. B. Henson, K. Müllen and G. C. Bazan, *Nat. Chem.*, 2012, **4**, 699–704.
24 X. Guo and A. Facchetti, *Nat. Mater.*, 2020, **19**, 922–928.
25 N. Huang, P. Wang and D. Jiang, *Nat. Rev. Mater.*, 2016, **1**, 16068.
26 R. Liu, K. T. Tan, Y. Gong, Y. Chen, Z. Li, S. Xie, T. He, Z. Lu, H. Yang and D. Jiang, *Chem. Soc. Rev.*, 2021, **50**, 120–242.
27 S.-Y. Ding and W. Wang, *Chem. Soc. Rev.*, 2013, **42**, 548–568.
28 X. Feng, X. Ding and D. Jiang, *Chem. Soc. Rev.*, 2012, **41**, 6010–6022.
29 D. Jiang, *Chem*, 2020, **6**, 2461–2483.
30 F. Yu, W. Liu, B. Li, D. Tian, J.-L. Zuo and Q. Zhang, *Angew. Chem., Int. Ed.*, 2019, **58**, 16101–16104.
31 F. Yu, W. Liu, S.-W. Ke, M. Kurmoo, J.-L. Zuo and Q. Zhang, *Nat. Commun.*, 2020, **11**, 5534.
32 A. F. Paterson, S. Singh, K. J. Fallon, T. Hodsden, Y. Han, B. C. Schroeder, H. Bronstein, M. Heeney, I. McCulloch and T. D. Anthopoulos, *Adv. Mater.*, 2018, **30**, 1801079.
33 H. Sun, X. Guo and A. Facchetti, *Chem*, 2020, **6**, 1310–1326.
34 X. Guo, A. Facchetti and T. J. Marks, *Chem. Rev.*, 2014, **114**, 8943–9021.
35 C. Wang, H. Dong, W. Hu, Y. Liu and D. Zhu, *Chem. Rev.*, 2012, **112**, 2208–2267.
36 Y. Zhao, Y. Guo and Y. Liu, *Adv. Mater.*, 2013, **25**, 5372–5391.
37 J. Zhou and B. Wang, *Chem. Soc. Rev.*, 2017, **46**, 6927–6945.
38 X. Zhao, P. Pachfule and A. Thomas, *Chem. Soc. Rev.*, 2021, **50**, 6871–6913.
39 J. Li, X. Jing, Q. Li, S. Li, X. Gao, X. Feng and B. Wang, *Chem. Soc. Rev.*, 2020, **49**, 3565–3604.
40 S. Muench, A. Wild, C. Friebe, B. Häupler, T. Janoschka and U. S. Schubert, *Chem. Rev.*, 2016, **116**, 9438–9484.
41 Y. Yusran, Q. Fang and V. Valtchev, *Adv. Mater.*, 2020, **32**, 2002038.
42 T. Sun, J. Xie, W. Guo, D.-S. Li and Q. Zhang, *Adv. Energy Mater.*, 2020, **10**, 1904199.
43 J. Wu, X. Rui, C. Wang, W.-B. Pei, R. Lau, Q. Yan and Q. Zhang, *Adv. Energy Mater.*, 2015, **5**, 1402189.
44 J. Wu, X. Rui, G. Long, W. Chen, Q. Yan and Q. Zhang, *Angew. Chem., Int. Ed.*, 2015, **54**, 7354–7358.
45 W. Yang, X. Du, J. Zhao, Z. Chen, J. Li, J. Xie, Y. Zhang, Z. Cui, Q. Kong, Z. Zhao, C. Wang, Q. Zhang and G. Cui, *Joule*, 2020, **4**, 1557–1574.
46 Z.-Q. Lin, J. Xie, B.-W. Zhang, J.-W. Li, J. Weng, R.-B. Song, X. Huang, H. Zhang, H. Li, Y. Liu, Z. J. Xu, W. Huang and Q. Zhang, *Nano Energy*, 2017, **41**, 117–127.
47 J. Xie, F. Yu, J. Zhao, W. Guo, H.-L. Zhang, G. Cui and Q. Zhang, *Energy Storage Mater.*, 2020, **33**, 283–289.
48 Y. Song, Q. Sun, B. Aguila and S. Ma, *Adv. Sci.*, 2019, **6**, 1801410.
49 N. Keller and T. Bein, *Chem. Soc. Rev.*, 2021, **50**, 1813–1845.
50 X. Liu, D. Huang, C. Lai, G. Zeng, L. Qin, H. Wang, H. Yi, B. Li, S. Liu, M. Zhang, R. Deng, Y. Fu, L. Li, W. Xue and S. Chen, *Chem. Soc. Rev.*, 2019, **48**, 5266–5302.
51 H. Wang, Z. Zeng, P. Xu, L. Li, G. Zeng, R. Xiao, Z. Tang, D. Huang, L. Tang, C. Lai, D. Jiang, Y. Liu, H. Yi, L. Qin, S. Ye, X. Ren and W. Tang, *Chem. Soc. Rev.*, 2019, **48**, 488–516.
52 (*a*) Y. H. Lee, M. Jang, M. Y. Lee, O. Y. Kweon and J. H. Oh, *Chem*, 2017, **3**, 724–763; (*b*) G. Sonmez, H. Meng, Q. Zhang and F. Wudl, *Adv. Funct. Mater.*, 2003, **13**, 726–731.
53 M. D. Allendorf, R. Dong, X. Feng, S. Kaskel, D. Matoga and V. Stavila, *Chem. Rev.*, 2020, **120**, 8581–8640.
54 S. Thomas, H. Li, R. R. Dasari, A. M. Evans, I. Castano, T. G. Allen, O. G. Reid, G. Rumbles, W. R. Dichtel, N. C. Gianneschi, S. R. Marder, V. Coropceanu and J.-L. Brédas, *Mater. Horiz.*, 2019, **6**, 1868–1876.
55 A. M. Evans, A. Giri, V. K. Sangwan, S. Xun, M. Bartnof, C. G. Torres-Castanedo, H. B. Balch, M. S. Rahn, N. P. Bradshaw, E. Vitaku, D. W. Burke, H. Li, M. J. Bedzyk, F. Wang, J.-L. Brédas, J. A. Malen, A. J. H. McGaughey, M. C. Hersam, W. R. Dichtel and P. E. Hopkins, *Nat. Mater.*, 2021, **20**, 1142–1148.
56 A. C. Arias, J. D. MacKenzie, I. McCulloch, J. Rivnay and A. Salleo, *Chem. Rev.*, 2010, **110**, 3–24.
57 H. Sirringhaus, *Adv. Mater.*, 2014, **26**, 1319–1335.
58 H. Ding, J. Li, G. Xie, G. Lin, R. Chen, Z. Peng, C. Yang, B. Wang, J. Sun and C. Wang, *Nat. Commun.*, 2018, **9**, 5234.
59 W. K. Haug, E. M. Moscarello, E. R. Wolfson and P. L. McGrier, *Chem. Soc. Rev.*, 2020, **49**, 839–864.
60 S. Xu and Q. Zhang, *Mater. Today Energy*, 2021, **20**, 100635.
61 D.-W. Zhang, M. Li and C.-F. Chen, *Chem. Soc. Rev.*, 2020, **49**, 1331–1343.
62 C. Yan, S. Barlow, Z. Wang, H. Yan, A. K. Y. Jen, S. R. Marder and X. Zhan, *Nat. Rev. Mater.*, 2018, **3**, 18003.
63 L. Lu, T. Zheng, Q. Wu, A. M. Schneider, D. Zhao and L. Yu, *Chem. Rev.*, 2015, **115**, 12666–12731.
64 T. Ma, E. A. Kapustin, S. X. Yin, L. Liang, Z. Zhou, J. Niu, L.-H. Li, Y. Wang, J. Su, J. Li, X. Wang, W. D. Wang, W. Wang, J. Sun and O. M. Yaghi, *Science*, 2018, **361**, 48–52.
65 H. A. Um, D. H. Lee, D. U. Heo, D. S. Yang, J. Shin, H. Baik, M. J. Cho and D. H. Choi, *ACS Nano*, 2015, **9**, 5264–5274.
66 Z.-F. Yao, Y.-Q. Zheng, J.-H. Dou, Y. Lu, Y.-F. Ding, L. Ding, J.-Y. Wang and J. Pei, *Adv. Mater.*, 2021, **33**, 2006794.
67 R. Freund, S. Canossa, S. M. Cohen, W. Yan, H. Deng, V. Guillerm, M. Eddaoudi, D. G. Madden, D. Fairen-Jimenez, H. Lyu, L. K. Macreadie, Z. Ji, Y. Zhang, B. Wang, F. Haase, C. Wöll, O. Zaremba, J. Andreo, S. Wuttke and C. S. Diercks, *Angew. Chem., Int. Ed.*, 2021, **60**, 2–31.
68 I. Hisaki, C. Xin, K. Takahashi and T. Nakamura, *Angew. Chem., Int. Ed.*, 2019, **58**, 11160–11170.
69 Q. Huang, W. Li, Z. Mao, H. Zhang, Y. Li, D. Ma, H. Wu, J. Zhao, Z. Yang, Y. Zhang, L. Gong, M. P. Aldred and Z. Chi, *Chem*, 2021, **7**, 1321–1332.
70 G. Chakraborty, I.-H. Park, R. Medishetty and J. J. Vittal, *Chem. Rev.*, 2021, **121**, 3751–3891.
71 L. Feng, K.-Y. Wang, G. S. Day, M. R. Ryder and H.-C. Zhou, *Chem. Rev.*, 2020, **120**, 13087–13133.
72 Y. Liu, Y. Wei, M. Liu, Y. Bai, X. Wang, S. Shang, J. Chen and Y. Liu, *Angew. Chem., Int. Ed.*, 2021, **60**, 2887–2891.

73 B. Gole, V. Stepanenko, S. Rager, M. Grüne, D. D. Medina, T. Bein, F. Würthner and F. Beuerle, *Angew. Chem., Int. Ed.*, 2018, **57**, 846–850.
74 C. B. Nielsen, M. Turbiez and I. McCulloch, *Adv. Mater.*, 2013, **25**, 1859–1880.
75 Z. Yi, S. Wang and Y. Liu, *Adv. Mater.*, 2015, **27**, 3589–3606.
76 J. Yang, H. Wang, J. Chen, J. Huang, Y. Jiang, J. Zhang, L. Shi, Y. Sun, Z. Wei, G. Yu, Y. Guo, S. Wang and Y. Liu, *Adv. Mater.*, 2017, **29**, 1606162.
77 M. Matsumoto, R. R. Dasari, W. Ji, C. H. Feriante, T. C. Parker, S. R. Marder and W. R. Dichtel, *J. Am. Chem. Soc.*, 2017, **139**, 4999–5002.
78 D. Bessinger, L. Ascherl, F. Auras and T. Bein, *J. Am. Chem. Soc.*, 2017, **139**, 12035–12042.
79 T. Lei, J.-Y. Wang and J. Pei, *Acc. Chem. Res.*, 2014, **47**, 1117–1126.
80 E. Wang, W. Mammo and M. R. Andersson, *Adv. Mater.*, 2014, **26**, 1801–1826.
81 L. Jiang, Y. Tian, T. Sun, Y. Zhu, H. Ren, X. Zou, Y. Ma, K. R. Meihaus, J. R. Long and G. Zhu, *J. Am. Chem. Soc.*, 2018, **140**, 15724–15730.
82 N. Sakai, J. Mareda, E. Vauthey and S. Matile, *Chem. Commun.*, 2010, **46**, 4225–4237.
83 S.-L. Suraru and F. Würthner, *Angew. Chem., Int. Ed.*, 2014, **53**, 7428–7448.
84 I. Osaka and K. Takimiya, *Adv. Mater.*, 2017, **29**, 1605218.
85 J. Yang, Y. Jiang, Z. Tu, Z. Zhao, J. Chen, Z. Yi, Y. Li, S. Wang, Y. Yi, Y. Guo and Y. Liu, *Adv. Funct. Mater.*, 2019, **29**, 1804839.
86 K.-J. Baeg, M. Caironi and Y.-Y. Noh, *Adv. Mater.*, 2013, **25**, 4210–4244.
87 K. Geng, T. He, R. Liu, S. Dalapati, K. T. Tan, Z. Li, S. Tao, Y. Gong, Q. Jiang and D. Jiang, *Chem. Rev.*, 2020, **120**, 8814–8933.
88 J. L. Segura, M. J. Mancheño and F. Zamora, *Chem. Soc. Rev.*, 2016, **45**, 5635–5671.
89 Y. Li, W. Chen, G. Xing, D. Jiang and L. Chen, *Chem. Soc. Rev.*, 2020, **49**, 2852–2868.
90 J. L. Segura, S. Royuela and M. Mar Ramos, *Chem. Soc. Rev.*, 2019, **48**, 3903–3945.
91 M. S. Lohse and T. Bein, *Adv. Funct. Mater.*, 2018, **28**, 1705553.
92 R. K. Sharma, P. Yadav, M. Yadav, R. Gupta, P. Rana, A. Srivastava, R. Zbořil, R. S. Varma, M. Antonietti and M. B. Gawande, *Mater. Horiz.*, 2020, **7**, 411–454.
93 B. Carsten, F. He, H. J. Son, T. Xu and L. Yu, *Chem. Rev.*, 2011, **111**, 1493–1528.
94 J.-R. Pouliot, F. Grenier, J. T. Blaskovits, S. Beaupré and M. Leclerc, *Chem. Rev.*, 2016, **116**, 14225–14274.
95 Z. Ni, H. Wang, H. Dong, Y. Dang, Q. Zhao, X. Zhang and W. Hu, *Nat. Chem.*, 2019, **11**, 271–277.
96 N. S. Gobalasingham and B. C. Thompson, *Prog. Polym. Sci.*, 2018, **83**, 135–201.
97 Y. Ran, Y. Guo and Y. Liu, *Mater. Horiz.*, 2020, **7**, 1955–1970.
98 G. Zhang, Y. Dai, Y. Liu, J. Liu, H. Lu, L. Qiu and K. Cho, *Polym. Chem.*, 2017, **8**, 3448–3456.
99 A. Onwubiko, W. Yue, C. Jellett, M. Xiao, H.-Y. Chen, M. K. Ravva, D. A. Hanifi, A.-C. Knall, B. Purushothaman, M. Nikolka, J.-C. Flores, A. Salleo, J.-L. Bredas, H. Sirringhaus, P. Hayoz and I. McCulloch, *Nat. Commun.*, 2018, **9**, 416.
100 A. M. Evans, L. R. Parent, N. C. Flanders, R. P. Bisbey, E. Vitaku, M. S. Kirschner, R. D. Schaller, L. X. Chen, N. C. Gianneschi and W. R. Dichtel, *Science*, 2018, **361**, 52–57.
101 M. Liu, K. Jiang, X. Ding, S. Wang, C. Zhang, J. Liu, Z. Zhan, G. Cheng, B. Li, H. Chen, S. Jin and B. Tan, *Adv. Mater.*, 2019, **31**, 1807865.
102 S. Karak, S. Kumar, P. Pachfule and R. Banerjee, *J. Am. Chem. Soc.*, 2018, **140**, 5138–5145.
103 S. Zhang, G. Cheng, L. Guo, N. Wang, B. Tan and S. Jin, *Angew. Chem., Int. Ed.*, 2020, **59**, 6007–6014.
104 M. Calik, T. Sick, M. Dogru, M. Döblinger, S. Datz, H. Budde, A. Hartschuh, F. Auras and T. Bein, *J. Am. Chem. Soc.*, 2016, **138**, 1234–1239.
105 D. Zhu, L. B. Alemany, W. Guo and R. Verduzco, *Polym. Chem.*, 2020, **11**, 4464–4468.
106 F. J. Uribe-Romo, J. R. Hunt, H. Furukawa, C. Klöck, M. O'Keeffe and O. M. Yaghi, *J. Am. Chem. Soc.*, 2009, **131**, 4570–4571.
107 T. Ma, J. Li, J. Niu, L. Zhang, A. S. Etman, C. Lin, D. Shi, P. Chen, L.-H. Li, X. Du, J. Sun and W. Wang, *J. Am. Chem. Soc.*, 2018, **140**, 6763–6766.
108 M. Liu, Q. Huang, S. Wang, Z. Li, B. Li, S. Jin and B. Tan, *Angew. Chem., Int. Ed.*, 2018, **57**, 11968–11972.
109 S. Wang, Z. Zhang, H. Zhang, A. G. Rajan, N. Xu, Y. Yang, Y. Zeng, P. Liu, X. Zhang, Q. Mao, Y. He, J. Zhao, B.-G. Li, M. S. Strano and W.-J. Wang, *Matter*, 2019, **1**, 1592–1605.
110 V. S. Vyas, F. Haase, L. Stegbauer, G. Savasci, F. Podjaski, C. Ochsenfeld and B. V. Lotsch, *Nat. Commun.*, 2015, **6**, 8508.
111 C. M. Thompson, G. Occhialini, G. T. McCandless, S. B. Alahakoon, V. Cameron, S. O. Nielsen and R. A. Smaldone, *J. Am. Chem. Soc.*, 2017, **139**, 10506–10513.
112 Z. Xie, B. Wang, Z. Yang, X. Yang, X. Yu, G. Xing, Y. Zhang and L. Chen, *Angew. Chem., Int. Ed.*, 2019, **58**, 15742–15746.
113 Z.-F. Pang, S.-Q. Xu, T.-Y. Zhou, R.-R. Liang, T.-G. Zhan and X. Zhao, *J. Am. Chem. Soc.*, 2016, **138**, 4710–4713.
114 S. B. Alahakoon, S. D. Diwakara, C. M. Thompson and R. A. Smaldone, *Chem. Soc. Rev.*, 2020, **49**, 1344–1356.
115 X. Chen, M. Addicoat, S. Irle, A. Nagai and D. Jiang, *J. Am. Chem. Soc.*, 2013, **135**, 546–549.
116 S. Kandambeth, D. B. Shinde, M. K. Panda, B. Lukose, T. Heine and R. Banerjee, *Angew. Chem., Int. Ed.*, 2013, **52**, 13052–13056.
117 X. Chen, M. Addicoat, E. Jin, L. Zhai, H. Xu, N. Huang, Z. Guo, L. Liu, S. Irle and D. Jiang, *J. Am. Chem. Soc.*, 2015, **137**, 3241–3247.
118 X. Guo, Y. Tian, M. Zhang, Y. Li, R. Wen, X. Li, X. Li, Y. Xue, L. Ma, C. Xia and S. Li, *Chem. Mater.*, 2018, **30**, 2299–2308.
119 A. Halder, S. Karak, M. Addicoat, S. Bera, A. Chakraborty, S. H. Kunjattu, P. Pachfule, T. Heine and R. Banerjee, *Angew. Chem., Int. Ed.*, 2018, **57**, 5797–5802.

120 S. B. Alahakoon, G. T. McCandless, A. A. K. Karunathilake, C. M. Thompson and R. A. Smaldone, *Chem. – Eur. J.*, 2017, **23**, 4255–4259.
121 Y. Li, Q. Chen, T. Xu, Z. Xie, J. Liu, X. Yu, S. Ma, T. Qin and L. Chen, *J. Am. Chem. Soc.*, 2019, **141**, 13822–13828.
122 E. Vitaku and W. R. Dichtel, *J. Am. Chem. Soc.*, 2017, **139**, 12911–12914.
123 N. Keller, D. Bessinger, S. Reuter, M. Calik, L. Ascherl, F. C. Hanusch, F. Auras and T. Bein, *J. Am. Chem. Soc.*, 2017, **139**, 8194–8199.
124 X. Wu, Y.-l. Hong, B. Xu, Y. Nishiyama, W. Jiang, J. Zhu, G. Zhang, S. Kitagawa and S. Horike, *J. Am. Chem. Soc.*, 2020, **142**, 14357–14364.
125 J.-K. Sun, Y. I. Sobolev, W. Zhang, Q. Zhuang and B. A. Grzybowski, *Nature*, 2020, **579**, 73–79.
126 L. Ascherl, E. W. Evans, M. Hennemann, D. Di Nuzzo, A. G. Hufnagel, M. Beetz, R. H. Friend, T. Clark, T. Bein and F. Auras, *Nat. Commun.*, 2018, **9**, 3802.
127 Y. Lv, Y. Li, G. Zhang, Z. Peng, L. Ye, Y. Chen, T. Zhang, G. Xing and L. Chen, *CCS Chem.*, 2021, **3**, 1773–1779.
128 D. Chen, W. Chen, G. Xing, T. Zhang and L. Chen, *Chem. – Eur. J.*, 2020, **26**, 8377–8381.
129 L. Bai, S. Z. F. Phua, W. Q. Lim, A. Jana, Z. Luo, H. P. Tham, L. Zhao, Q. Gao and Y. Zhao, *Chem. Commun.*, 2016, **52**, 4128–4131.
130 H. Li, P. Shao, S. Chen, G. Li, X. Feng, X. Chen, H.-J. Zhang, J. Lin and Y.-B. Jiang, *J. Am. Chem. Soc.*, 2020, **142**, 3712–3717.
131 D. Beaudoin, T. Maris and J. D. Wuest, *Nat. Chem.*, 2013, **5**, 830–834.
132 T. Ma, L. Wei, L. Liang, S. Yin, L. Xu, J. Niu, H. Xue, X. Wang, J. Sun, Y.-B. Zhang and W. Wang, *Nat. Commun.*, 2020, **11**, 6128.
133 Y.-B. Zhang, J. Su, H. Furukawa, Y. Yun, F. Gándara, A. Duong, X. Zou and O. M. Yaghi, *J. Am. Chem. Soc.*, 2013, **135**, 16336–16339.
134 C. Gao, J. Li, S. Yin, G. Lin, T. Ma, Y. Meng, J. Sun and C. Wang, *Angew. Chem., Int. Ed.*, 2019, **58**, 9770–9775.
135 H.-S. Xu, Y. Luo, X. Li, P. Z. See, Z. Chen, T. Ma, L. Liang, K. Leng, I. Abdelwahab, L. Wang, R. Li, X. Shi, Y. Zhou, X. F. Lu, X. Zhao, C. Liu, J. Sun and K. P. Loh, *Nat. Commun.*, 2020, **11**, 1434.
136 B. J. Smith, L. R. Parent, A. C. Overholts, P. A. Beaucage, R. P. Bisbey, A. D. Chavez, N. Hwang, C. Park, A. M. Evans, N. C. Gianneschi and W. R. Dichtel, *ACS Cent. Sci.*, 2017, **3**, 58–65.
137 A. M. Evans, I. Castano, A. Brumberg, L. R. Parent, A. R. Corcos, R. L. Li, N. C. Flanders, D. J. Gosztola, N. C. Gianneschi, R. D. Schaller and W. R. Dichtel, *J. Am. Chem. Soc.*, 2019, **141**, 19728–19735.
138 L. Liang, Y. Qiu, W. D. Wang, J. Han, Y. Luo, W. Yu, G.-L. Yin, Z.-P. Wang, L. Zhang, J. Ni, J. Niu, J. Sun, T. Ma and W. Wang, *Angew. Chem., Int. Ed.*, 2020, **59**, 17991–17995.
139 P. Sonar, S. P. Singh, Y. Li, M. S. Soh and A. Dodabalapur, *Adv. Mater.*, 2010, **22**, 5409–5413.
140 J. S. Ha, K. H. Kim and D. H. Choi, *J. Am. Chem. Soc.*, 2011, **133**, 10364–10367.
141 J. Lee, A. R. Han, J. Kim, Y. Kim, J. H. Oh and C. Yang, *J. Am. Chem. Soc.*, 2012, **134**, 20713–20721.
142 B. He, A. B. Pun, D. Zherebetskyy, Y. Liu, F. Liu, L. M. Klivansky, A. M. McGough, B. A. Zhang, K. Lo, T. P. Russell, L. Wang and Y. Liu, *J. Am. Chem. Soc.*, 2014, **136**, 15093–15101.
143 H. N. Tsao, D. M. Cho, I. Park, M. R. Hansen, A. Mavrinskiy, D. Y. Yoon, R. Graf, W. Pisula, H. W. Spiess and K. Müllen, *J. Am. Chem. Soc.*, 2011, **133**, 2605–2612.
144 M. Zhang, H. N. Tsao, W. Pisula, C. Yang, A. K. Mishra and K. Müllen, *J. Am. Chem. Soc.*, 2007, **129**, 3472–3473.
145 H. N. Tsao, D. Cho, J. W. Andreasen, A. Rouhanipour, D. W. Breiby, W. Pisula and K. Müllen, *Adv. Mater.*, 2009, **21**, 209–212.
146 J. Li, Y. Zhao, H. S. Tan, Y. Guo, C.-A. Di, G. Yu, Y. Liu, M. Lin, S. H. Lim, Y. Zhou, H. Su and B. S. Ong, *Sci. Rep.*, 2012, **2**, 754.
147 Y.-Z. Dai, N. Ai, Y. Lu, Y.-Q. Zheng, J.-H. Dou, K. Shi, T. Lei, J.-Y. Wang and J. Pei, *Chem. Sci.*, 2016, **7**, 5753–5757.
148 Y. Wang, T. Hasegawa, H. Matsumoto and T. Michinobu, *J. Am. Chem. Soc.*, 2019, **141**, 3566–3575.
149 X. Guo, J. Quinn, Z. Chen, H. Usta, Y. Zheng, Y. Xia, J. W. Hennek, R. P. Ortiz, T. J. Marks and A. Facchetti, *J. Am. Chem. Soc.*, 2013, **135**, 1986–1996.
150 T. Lei, J.-H. Dou, X.-Y. Cao, J.-Y. Wang and J. Pei, *Adv. Mater.*, 2013, **25**, 6589–6593.
151 Z. Fei, P. Pattanasattayavong, Y. Han, B. C. Schroeder, F. Yan, R. J. Kline, T. D. Anthopoulos and M. Heeney, *J. Am. Chem. Soc.*, 2014, **136**, 15154–15157.
152 T. Lei, Y. Cao, X. Zhou, Y. Peng, J. Bian and J. Pei, *Chem. Mater.*, 2012, **24**, 1762–1770.
153 L. Ying, B. B. Y. Hsu, H. Zhan, G. C. Welch, P. Zalar, L. A. Perez, E. J. Kramer, T.-Q. Nguyen, A. J. Heeger, W.-Y. Wong and G. C. Bazan, *J. Am. Chem. Soc.*, 2011, **133**, 18538–18541.
154 L. Ying, F. Huang and G. C. Bazan, *Nat. Commun.*, 2017, **8**, 14047.
155 R. Rieger, D. Beckmann, A. Mavrinskiy, M. Kastler and K. Müllen, *Chem. Mater.*, 2010, **22**, 5314–5318.
156 T. Lei, Y. Cao, Y. Fan, C.-J. Liu, S.-C. Yuan and J. Pei, *J. Am. Chem. Soc.*, 2011, **133**, 6099–6101.
157 M. Wang, M. Ford, H. Phan, J. Coughlin, T.-Q. Nguyen and G. C. Bazan, *Chem. Commun.*, 2016, **52**, 3207–3210.
158 Y. Wang, Z. Yan, H. Guo, M. A. Uddin, S. Ling, X. Zhou, H. Su, J. Dai, H. Y. Woo and X. Guo, *Angew. Chem., Int. Ed.*, 2017, **56**, 15304–15308.
159 W. Lee, G.-H. Kim, S.-J. Ko, S. Yum, S. Hwang, S. Cho, Y.-H. Shin, J. Y. Kim and H. Y. Woo, *Macromolecules*, 2014, **47**, 1604–1612.
160 T. Lei, J.-H. Dou and J. Pei, *Adv. Mater.*, 2012, **24**, 6457–6461.
161 J. Mei and Z. Bao, *Chem. Mater.*, 2014, **26**, 604–615.
162 J. Lee, A. R. Han, H. Yu, T. J. Shin, C. Yang and J. H. Oh, *J. Am. Chem. Soc.*, 2013, **135**, 9540–9547.
163 B. Kang, R. Kim, S. B. Lee, S.-K. Kwon, Y.-H. Kim and K. Cho, *J. Am. Chem. Soc.*, 2016, **138**, 3679–3686.

164 J. Yao, C. Yu, Z. Liu, H. Luo, Y. Yang, G. Zhang and D. Zhang, *J. Am. Chem. Soc.*, 2016, **138**, 173–185.
165 Y. Yang, Z. Liu, G. Zhang, X. Zhang and D. Zhang, *Adv. Mater.*, 2019, **31**, 1903104.
166 I. Kang, H.-J. Yun, D. S. Chung, S.-K. Kwon and Y.-H. Kim, *J. Am. Chem. Soc.*, 2013, **135**, 14896–14899.
167 M. S. Chen, O. P. Lee, J. R. Niskala, A. T. Yiu, C. J. Tassone, K. Schmidt, P. M. Beaujuge, S. S. Onishi, M. F. Toney, A. Zettl and J. M. J. Fréchet, *J. Am. Chem. Soc.*, 2013, **135**, 19229–19236.
168 Z. Wang, Z. Liu, L. Ning, M. Xiao, Y. Yi, Z. Cai, A. Sadhanala, G. Zhang, W. Chen, H. Sirringhaus and D. Zhang, *Chem. Mater.*, 2018, **30**, 3090–3100.
169 Y.-J. Heo, H.-G. Jeong, J. Kim, B. Lim, J. Kim, Y. Kim, B. Kang, J.-M. Yun, K. Cho and D.-Y. Kim, *ACS Appl. Mater. Interfaces*, 2020, **12**, 49886–49894.
170 T. Lei, X. Xia, J.-Y. Wang, C.-J. Liu and J. Pei, *J. Am. Chem. Soc.*, 2014, **136**, 2135–2141.
171 S. Yum, T. K. An, X. Wang, W. Lee, M. A. Uddin, Y. J. Kim, T. L. Nguyen, S. Xu, S. Hwang, C. E. Park and H. Y. Woo, *Chem. Mater.*, 2014, **26**, 2147–2154.
172 Y. Gao, X. Zhang, H. Tian, J. Zhang, D. Yan, Y. Geng and F. Wang, *Adv. Mater.*, 2015, **27**, 6753–6759.
173 M. Wang, M. J. Ford, A. T. Lill, H. Phan, T.-Q. Nguyen and G. C. Bazan, *Adv. Mater.*, 2017, **29**, 1603830.
174 Y. Sun, Y. Zhang, Y. Ran, L. Shi, Q. Zhang, J. Chen, Q. Li, Y. Guo and Y. Liu, *J. Mater. Chem. C*, 2020, **8**, 15168–15174.
175 Y. Gao, Y. Deng, H. Tian, J. Zhang, D. Yan, Y. Geng and F. Wang, *Adv. Mater.*, 2017, **29**, 1606217.
176 K. Rahimi, I. Botiz, N. Stingelin, N. Kayunkid, M. Sommer, F. P. V. Koch, H. Nguyen, O. Coulembier, P. Dubois, M. Brinkmann and G. Reiter, *Angew. Chem., Int. Ed.*, 2012, **51**, 11131–11135.
177 J. H. Kim, D. H. Lee, D. S. Yang, D. U. Heo, K. H. Kim, J. Shin, H.-J. Kim, K.-Y. Baek, K. Lee, H. Baik, M. J. Cho and D. H. Choi, *Adv. Mater.*, 2013, **25**, 4102–4106.
178 Y. Yao, H. Dong, F. Liu, T. P. Russell and W. Hu, *Adv. Mater.*, 2017, **29**, 1701251.
179 Z. Ni, H. Dong, H. Wang, S. Ding, Y. Zou, Q. Zhao, Y. Zhen, F. Liu, L. Jiang and W. Hu, *Adv. Mater.*, 2018, **30**, 1704843.

